Supplementary Information for:

How Ag Nanospheres are Transformed into AgAu Nanocages

Liane M. Moreau[1,5], Charles A. Schurman[2,5], Sumit Kewalramani[1,5], Mohammad M. Shahjamali[3,5], Chad A. Mirkin*[1,2,3,5], and Michael J. Bedzyk*[1,4,5]

[1]Department of Materials Science and Engineering, [2]Department of Biomedical Engineering, [3]Department of Chemistry, [4]Department of Physics and Astronomy, and [5]International Institute for Nanotechnology, Northwestern University, Evanston, IL 60208

Extended Methods

Nanoparticle Synthesis

$HAuCl_4$ salt (Sigma-Aldrich) was dissolved in NANOpure™ water to prepare a 0.1 mM solution. This Au solution was then titrated into a vial of ~3 pM (determined from XRF) citrate capped silver spheres (nominal diameter 20 nm, Ted Pella) using a syringe pump at a rate of 20 ml/hr at room temperature. Different volumes of Au solution were added to each sample of Ag particles in order to halt the reaction at different stages of transformation. After titration, samples were stirred for several minutes in order to ensure reaction completion. Transformed particles were isolated via centrifugation (21130 g for 20 mins) and the supernatant was removed to eliminate free ions from solution. Particle pellets were resuspended in 2 mL of NANOpure™ water and centrifugation was repeated to remove excess Au^{3+} ions. After UV-vis measurements to probe the optical absorption spectra and localized surface plasmon resonance peak position, samples were isolated via centrifugation a final time and resuspended in 100 µL NANOpure™ water. UV-vis spectra taken before and after this centrifugation step show that the particles maintain their nanocage structure and are not destroyed during the high-speed centrifugation (Fig. S1). 20 µL of both a 1% (w/w) SDS and a 0.1% (w/w) Tween (Sigma-Aldrich) were added to samples to act as surfactant and to ensure longevity of particles.

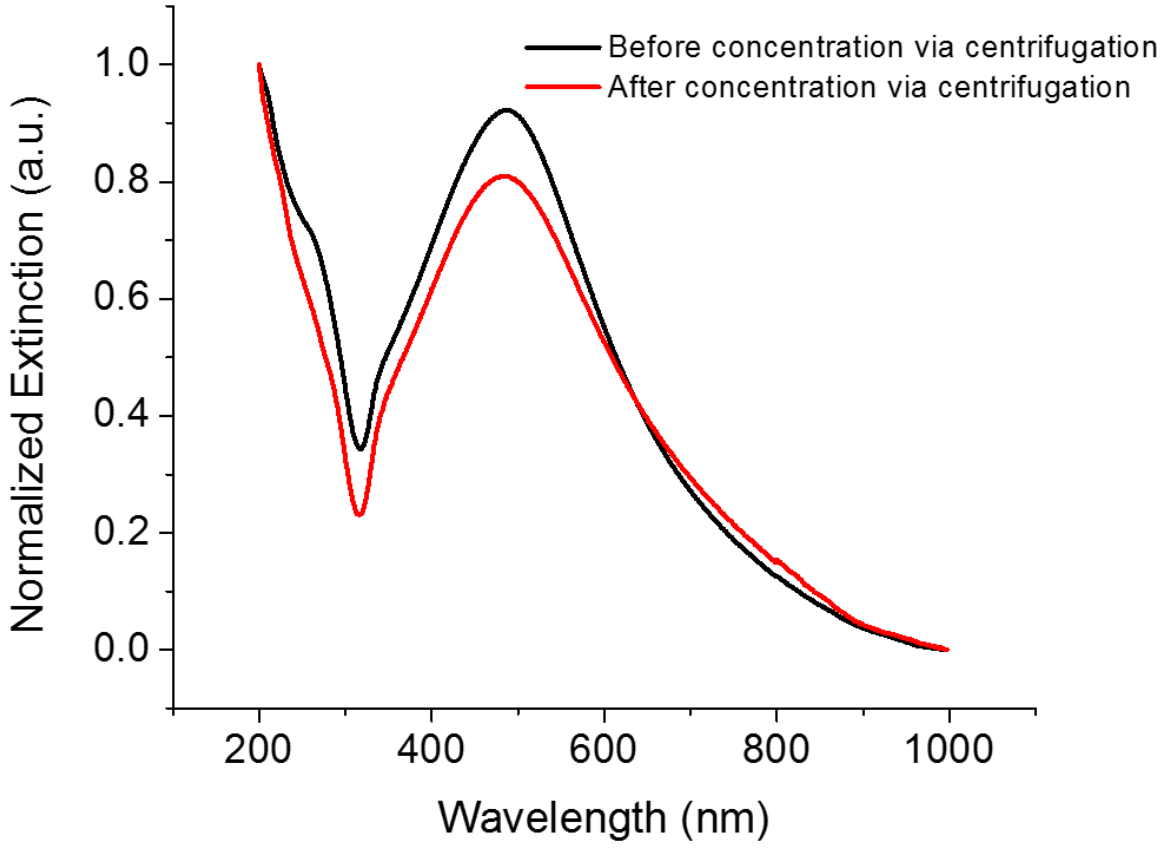

Figure S1. Partially transformed AgAu nanocage sample before and after concentration for x-ray measurements. Normalized UV-vis spectra of ~25 % Au nanocages before and after undergoing concentration via centrifugation for x-ray measurements show that the LSPR peak position and overall spectral features are maintained. This suggests that the particles do not collapse during the high-speed centrifugation step.

TEM Size Analysis

Nanoparticle size was determined by a statistical analysis of TEM images using the ImageJ particle counter software. The average number of particles used in the analysis was 113, with a minimum of 50 particles and a maximum of 250 particles at the extremes. Results of this analysis, along with particle size as determined from SAXS, are shown in Fig. S10.

X-Ray Fluorescence

X-ray fluorescence (XRF) data from the Ag Kα and Au L fluorescence lines were collected along with XAFS data at sector 10BM-B at the Argonne National Laboratory Advanced Photon Source (APS). The corrected fluorescence intensities of the Ag Kα and Au Lα lines were used to determine the relative Au and Ag atomic percentages present in the isolated nanoparticle samples, with varying solution concentrations of $HAuCl_4$ added. Samples were contained in 3 mm (nominal, Charles Supper) inner diameter cylindrical quartz capillaries placed such that the capillary long axis was at a 45° angle with the detector normal and the incident x-ray beam. The XRF photons were collected in the horizontal plane with the detector at ~ 90° relative to the incident beam direction to minimize the intensity due to elastically scattered X-rays. XRF data was collected at an incident energy of 26.014 keV using a four-element Vortex ME-4 silicon drift diode detector. A schematic of the measurement setup is shown in Figure S2.

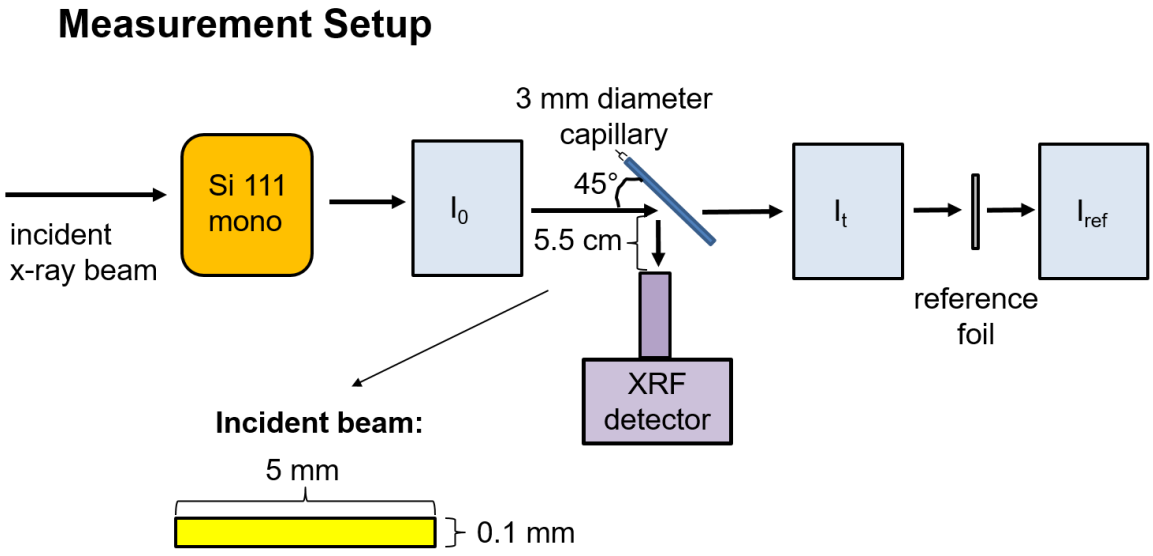

Figure S2. XRF and XAFS measurement setup. I_0 measures the incident and I_t the transmitted x-ray intensity. I_{ref} is used to measure the reference XAFS spectrum. The reference foil is either Ag or Au depending on the edge being scanned.

In order to determine the starting nanoparticle concentration, absolute number of Ag atoms in the starting nanoparticle solution as well as isolated supernatant were determined using XRF data collected at APS sector 5BM-D of DND-CAT at an incident

energy of 26.014 keV. This was accomplished through including an internal Yb standard of known concentration (Sigma Aldrich) in the nanoparticle solution. Ag nanoparticles were contained in 2 mm quartz capillaries and placed at a 45° angle from two four-element Vortex ME-4 silicon drift diode detectors placed on either side of the sample.

Qualitatively, we observe (Figure S3) that with increasing $HAuCl_4$ incorporated into solution, the Au Lα fluorescence intensity increases while the higher energy Ag Kα fluorescence intensity decreases as would be expected. Quantitative analysis of the Au and Ag relative atomic percentages were conducted using areas under the Ag Kα (22.163 keV) and Au Lα (9.705 keV) fluorescence lines, with peaks fit to a Gaussian function after background subtraction. Elemental XRF cross sections,[1] detector efficiency, and attenuation due to solvent media were taken into account in determining the Ag/Au ratio. (Note that self-absorption by the metal NPs could be neglected due to their low μM atomic concentrations in the solvent.) The beam size was 0.1 mm (vertical) x 5 mm (horizontal). Therefore, for attenuation correction for Ag Kα and Au Lα X-rays coming from the 2 or 3 mm diameter cylinder of water, we neglected the vertical beam size. The path lengths and attenuation corrections for fluorescence X-rays were calculated by dividing the horizontal illuminated 10 - 15 mm^2 area into 121 differential emission elements arranged on a 2D lattice. The corrected intensities yielded the same atomic fraction for Au when Au Lα, Au Lβ or Au Lγ fluorescence lines were used, validating this correction procedure.

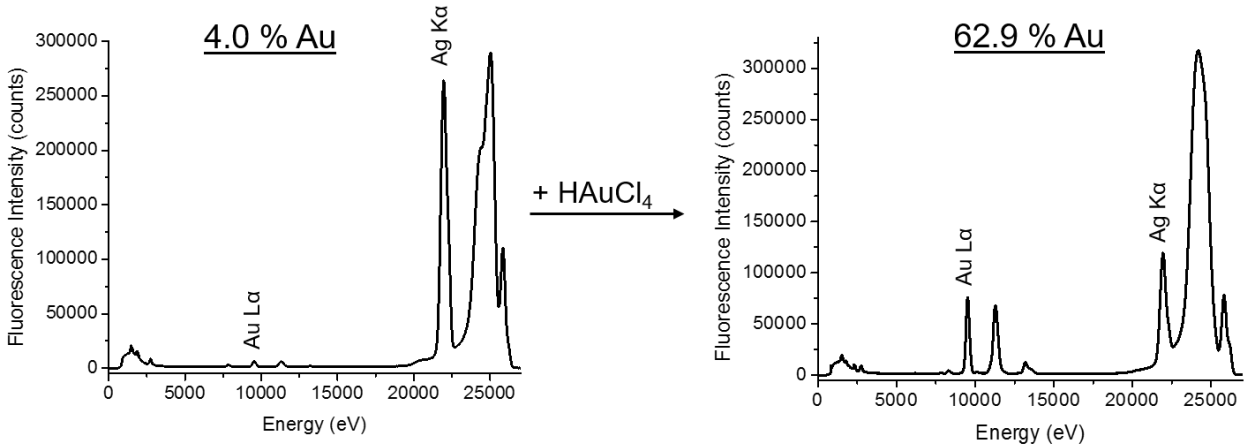

Figure S3. X-Ray fluorescence spectra. Qualitatively, it can be observed that both Au and Ag fluorescence lines are present in the raw XRF spectra. From low amounts to

higher amounts of $HAuCl_4$ added (left to right), the Au L fluorescence lines increase in intensity, while the Ag Kα intensity decreases. From quantitative analysis, the relative atomic percentages were determined to be 4.0 % Au (left) to 62.9 % Au (right). This is reasonable considering the amount of $HAuCl_4$ introduced into solution.

X-ray Scattering

X-ray scattering measurements were performed using 10.00 keV X-rays at beamline 5ID-D of the Advanced Photon Source (APS) at the Argonne National Laboratory. The aqueous nanoparticle dispersions were placed in a quartz capillary tube (inner diameter ~ 1.5 mm), which was embedded in a flow cell. To avoid radiation damage, the aqueous solutions were continuously flowed (unidirectional flow) at a rate of 2 mm/s during data collection. Furthermore, a fast shutter was used such that the samples were exposed to X-rays only for the data collection periods. The X-ray spot size at the sample position was ~ 0.25 mm (H) × 0.25 mm (V). The incident flux was ~ 10^{12} photons/s. The scattered intensity was collected using a Rayonix CCD area detectors, which was placed at 7502.0 mm (range: q = 0.015 – 0.9 nm^{-1}) from the sample, where $q = 4\pi sin\theta/\lambda$ is the scattering vector magnitude defined by scattering angle, 2θ, and wavelength, λ. The flight path between the sample flow cell and the detector was evacuated.

For each nanoparticle sample, five measurements were performed with an exposure time of 0.5 s each. To estimate background scattering, prior to measurements on every nanoparticle sample, five sets of data for empty capillary and capillary filled with water were collected with an exposure time of 10 s each. To account for fluctuations in the incident beam intensity and changes in the absorption of X-rays for different samples, the incident and the transmitted beam intensities were monitored using an ion chamber just before the sample and a pin diode embedded in the beam stop just in front of the SAXS detector. Transmission, detector solid angle and X-ray polarization corrections were applied to measured intensities before performing the azimuthal integration for extracting the 1D intensity profiles. The data shown (figure S6) is the intensity above the background scattering from capillary and pure water, and is an average of five measurements.

X-ray Scattering Data Analysis

The measured intensity profile $I(q)$ could be reasonably described by assuming a spherical core-shell model for the form factor [$F(q)$] of the Ag and Ag/Au alloy nanoparticles.[2] Specifically,

$$F(q) = \frac{4\pi}{q^3}[(\rho_c - \rho_s)\{\sin[qR_c] - qR_c\cos[qR_c]\} + (\rho_s - \rho_{sol})\{\sin[q(R_c + T_s)] - q(R_c + T_s)\cos[q(R_c + T_s)]\}] \quad \text{(S1)}$$

Here, R_c is the radius of the hollowed-out core for the Ag/Au alloy nanoparticles. For unalloyed pure Ag nanoparticles, R_c = 0. The electron density ρ_c for the hollowed out core is assumed to be the same as that for water solvent ($\rho_c = \rho_{sol}$ = 334 e^-/nm^3). T_s is the thickness of the metallic shell, and ρ_s is the electron density for the shell. And

$$I(q) = \frac{N}{V} r_e^2 \langle [F(q)]^2 \rangle + bkg \quad \text{(S2)}$$

To take into account the polydispersity (PD) of nanoparticles, the scattered intensity from an isolated nanoparticle $[F(q)]^2$ is averaged over a Schulz distribution[3] for particle sizes to yield $\langle [F(q)]^2 \rangle$. Here, the ratio of core radius and the shell thickness [R_c/T_s] is assumed to be a constant for all the Ag/Au alloy particles in a given solution. In Eq. S2, r_e is the classical electron radius and N/V is the number density of nanoparticles in the solution. The constant *bkg* represents any additional background scattering apart from those from the quartz capillary and water. For example, scattering from excess solution reagents, such as sodium citrate surfactant and $HAuCl_4$ salt. Overall, six parameters were used to fit the measured $I(q)$ for Ag/Au alloy nanoparticles. These were R_c, [R_c/T_s], ρ_s, Z, N/V *and bkg.* Z is the Schulz distribution parameter, which defines polydispersity: $\%PD = \frac{100}{\sqrt{Z+1}}$.

The Ag/Au alloy nanoparticles are not perfect spheres. TEM micrographs show nanoparticles with corrugated surfaces. Therefore, the spherical core-shell model is a simplified representation of these nanoparticles. As can be seen in Figs. S6.1-15 the core-shell model fits to the experimental $I(q)$ profiles are nearly perfect over a region 0.01< q < 0.09 $Å^{-1}$ that includes the form factor minimum and the maximum. Therefore it is reasonable to accept the fits from this method and the structural parameters derived

thereof despite small deviations, which are accounted for within the subsequent error analysis.

X-Ray Absorption Fine Structure

XAFS spectra at the Au L_3 edge and Ag K edge (11.919 keV and 25.514 keV) were collected at MR-CAT sector 10BM-B of the APS. Energy scans were taken over a range from -150 eV to 600 eV with respect to the absorption edge using a Si(111) monochromator. XAFS spectra were collected in fluorescence mode using a four-element Vortex ME-4 Silicon drift diode fluorescence detector, calibrated with an Au or Ag metal foil standard. Ag or Au foil spectra were simultaneously collected along with the nanoparticle samples, as shown in Fig. S2, in order to ensure calibration and compare absorption edge positions. Samples were concentrated via centrifugation to μM concentrations of Au/Ag atoms and placed in 3 mm inner diameter quartz capillary tubes, positioned 45 degrees with respect to both the incident x-ray beam and the fluorescence detector. To improve statistics, a minimum of five half-hour scans at 4 spectra/scan were averaged. Self-absorption was not a concern in the measurement, because of the low concentration of the element of interest (Au or Ag).

XAFS data was processed using ATHENA and ARTEMIS software, part of the IFEFFIT package.[4] Theoretical crystals structures were imported and converted to scattering pathways using ATOMS.[5] Absorption edge energy was determined from the maximum of the first derivative in the absorption data and the background was subtracted using the AUTOBK algorithm.[6] The EXAFS region (greater than 100 eV above the absorption edge)[7] was normalized and a k-weight of 2 was chosen in order to provide an even spectrum throughout the region of interest (2 – 12 $Å^{-1}$). EXAFS spectra were modeled according to the EXAFS equation, a simplified version of which is:[7-8, 9, 10]

$$\chi(k) = \sum_{\Gamma}\left[\frac{N_{\Gamma} S_0^2 F_{\Gamma}(k)}{2kR_{\Gamma}^2} e^{-2k^2\sigma_{\Gamma}^2} e^{-2R_{\Gamma}/\lambda(k)} \times \sin\left(2kR_{\Gamma} + \phi_{\Gamma}(k)\right)\right] \qquad \text{(S3)}$$

Where Γ is the summation over the individual scattering pathways included in the model, k is the photoelectron wavevector, $F_\Gamma(k)$ is the scattering amplitude, $\lambda(k)$ is the mean free path of inelastically-scattered photoelectrons and $\Phi(k)$ is the phase shift,

which is calculated as a function of the absorbing and scattering atom using the ARTEMIS software. S_0^2, the amplitude reduction factor, was set to the value extracted from fitting a bulk Au or Ag foil as applicable. This enables a more accurate determination of the coordination number.[9] Degeneracy (N_r), half-path length (R_r), energy shift parameter (E_0), and mean-squared disorder (σ_r^2), which includes contributions from structural and thermal disorder (Debye-Waller factor),[7] were adjusted to determine the best fit model. Fits with values for these variables outside the realm of physical reasonability (i.e. negative mean-squared disorder) were restricted. ΔE_0 was fixed to a single variable for all pathways with the same absorbing and scattering element in order to limit the number of variables, as ΔE_0 values should be nearly equal for similar bonds within the structure.[11]

Goodness of fit parameters for the models were evaluated using minimization of the statistical R-factor parameter and error bars for individual parameters were estimated to one sigma (~ 68% confidence level) from the R-space spectrum. Spectra were fit first in k-space, then evaluated in R-space and q-space, in order to ensure that the best fit to the raw data in k-space was translatable to the other fitting spaces. Individual fitting models and a summary of both fitting and goodness of fit parameters are included in figure S16.

Supplementary Results

Energy Dispersive X-Ray Spectroscopy

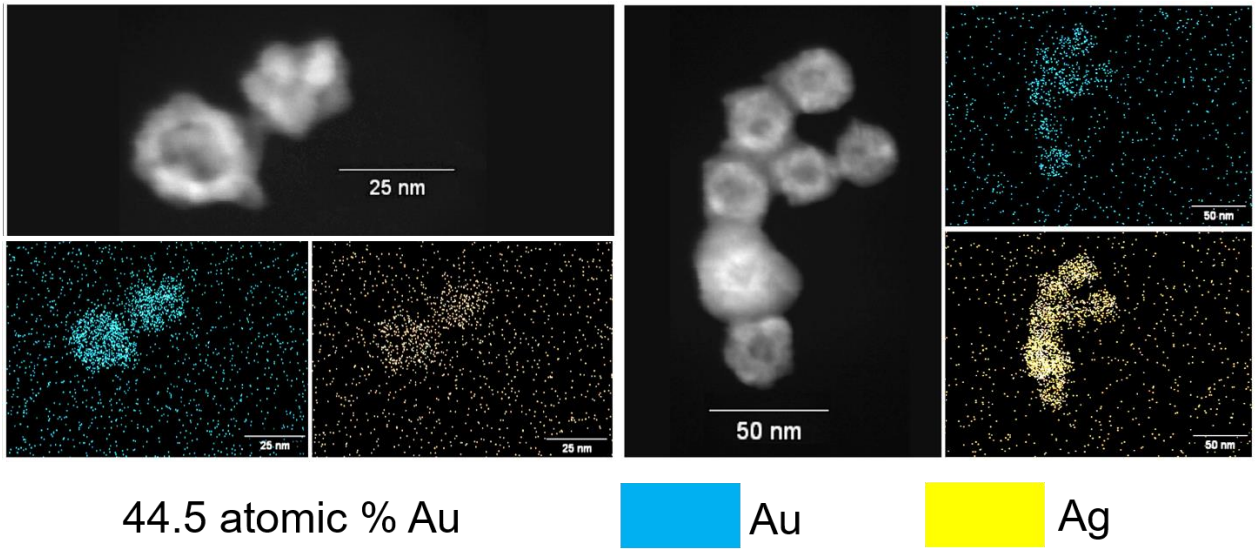

Figure S4. EDX mapping of Au and Ag spatial distribution. EDX mapping of nanoparticles that have been partially titrated with $HAuCl_4$ shows that both the Ag signal (yellow) and Au signal (blue) are distributed evenly throughout the nanoparticles. Given the resolution of EDX is ~ 2 nm and we observe local clustering from XAFS coordination numbers, this suggests that the local Au and Ag clusters within the particles are < 2 nm. The particles are atomically segregated, but alloyed at the nanoscale.

XAFS-derived Ag and Au cluster size in AgAu nanoparticles

The size of Ag and Au domains in the AgAu nanoparticles were estimated using the procedure extablished by Calvin et. al, which makes use of first-shell XAFS-derived coordination numbers to estimate particle size (Eq. S4), where N_{nano} is the XAFS-derived coordination number for Au-Au or Ag-Ag within the particles, N_{bulk} = 12, r is the nearest-neighbor distance (2.884 Å) and R is the radius of the Au or Ag cluster size.[12]

$$N_{nano} = [1 - \frac{3}{4}\left(\frac{r}{R}\right) + \frac{1}{16}\left(\frac{r}{R}\right)^3]N_{bulk} \quad \text{(S4)}$$

As the presence of Ag and Au clustering as been observed from the deviation of CNs from the case of alloy homogeneity (Fig. 5), this approach can be used to estimate cluster size. The results of this analysis are shown in Fig. S5 and show that the local clustering of Ag and Au is solely at the atomic scale (< 1 nm).

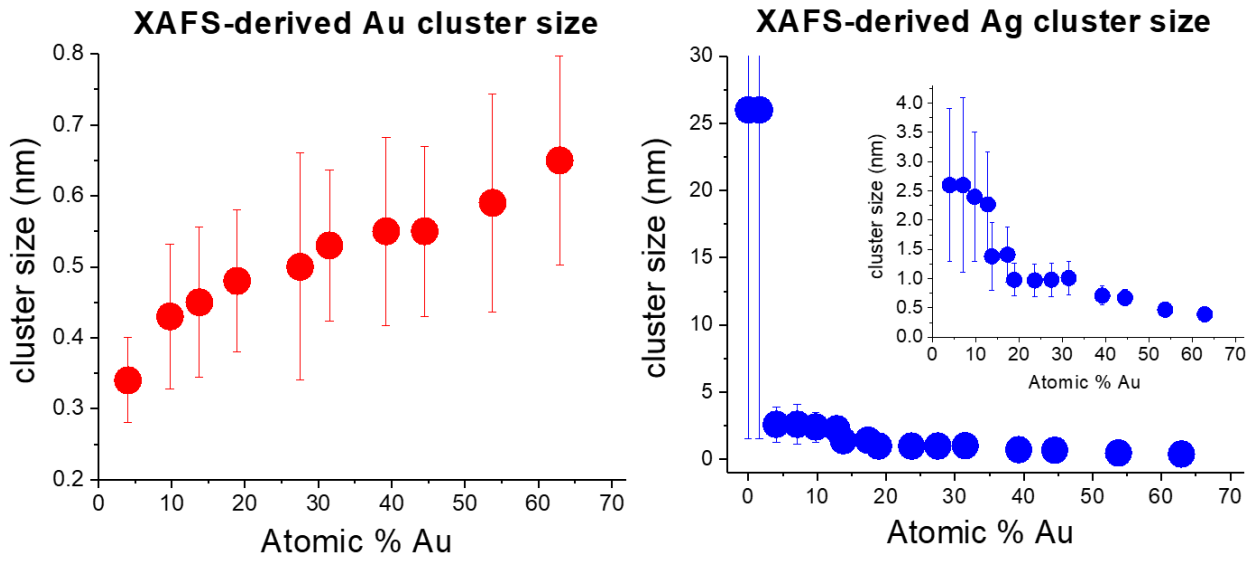

Figure S5. Ag and Au cluster size in AgAu nanoparticles. Au (left, red) and Ag (right, blue) sizes of Ag and Au regions within the atomically-segregated particles were estimated from XAFS first-shell coordination numbers. Throughout, the Au cluster radius is < 1 nm and after the initial transformation stages, the Ag cluster radius is also < 1nm, which agrees with EDX data (Figure S4) which shows that the AgAu nanocages are alloys on the nanoscale. Ag and Au regions are limited to the local atomic scale.

Quantitative Investigation of Ag:Au Exchange Ratio

The Ag:Au exchange ratio was calculated by comparing the ratio of the number of Ag atoms lost from the total number of Ag atoms originally in the nanoparticles (determined by XRF) to the number of Au atoms incorporated into the nanoparticle (number of Au atoms added minus the percentage unreacted in the supernatant (determined from ICP-MS)):

$$\frac{\textbf{number of Ag atoms lost from particles}}{\textbf{number of Au atoms incorporated into particles}}$$

Au atomic %	Ag:Au Replacement Ratio
1.6	0.5 ± 0.1

4.0	**2.1 ± 0.4**
7.1	**3.2 ± 0.5**
9.8	**3.0 ± 0.4**
12.8	**2.9 ± 0.4**
13.8	**2.4 ± 0.3**
17.4	**2.1 ± 0.3**
18.9	**1.5 ± 0.2**
23.7	**2.0 ± 0.3**
27.5	**2.0 ± 0.2**
31.5	**1.6 ± 0.2**
39.3	**1.6 ± 0.2**
44.5	**1.6 ± 0.2**
53.8	**1.7 ± 0.1**
62.9	**1.7 ± 0.2**

Table S1. Ag:Au replacement ratio as a function of $HAuCl_4$ addition. This table reveals the result that the exchange of Ag with Au atoms deviates from the expected 3:1 ratio from the Galvanic reaction alone. Rather, initially the Ag:Au replacement ratio is 1/2, indicating the addition of 2 Au atoms onto the nanoparticle surface for every Ag atom removed. The replacement ratio then increases to mimic the 3:1 ratio and again decreases as the reaction progresses until the nanoparticles begin to deteriorate.

Single-Shell SAXS Spectra + Fits

SAXS Error Reporting

The error bars on the measured data (Figs. S6 and S8, green) are smaller than the marker sizes. Positive and negative error values for parameters shown in the tables below were calculated based on $\Delta\chi^2 = 1$ maps and represent 68 % confidence intervals. The average polydispersity in the total nanoparticle size was 21 % with a std. dev. of 6 % between samples from different batches. The confidence intervals on the electron density are estimated in a different manner as described next. To fit the data, we multiplied by an overall scale factor, which ideally represents the product of the sample concentration multiplied by the square of the classical electron radius. The value of the scale factor over the whole series of samples showed a variation of ± 50 %. In our specific case of core-shell particles with the same electron density in the core as the surrounding bulk

$$I \propto scale\ factor * (\rho - \rho_w)^2 \quad \text{(S5)}$$

Assuming that the concentration of particles was constant throughout the measurements, the error in scale factor corresponds to a maximum of 25 % error in the electron density of the shell.

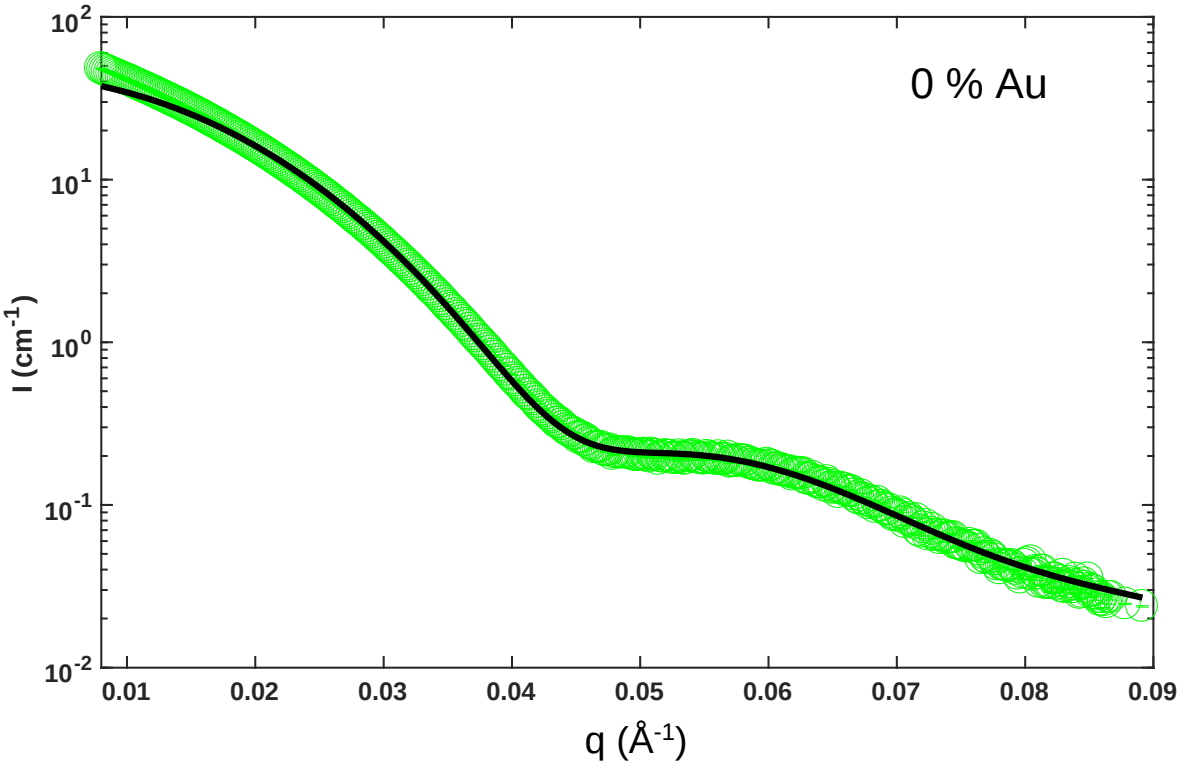

Total Particle Radius (nm)	Core Radius:Shell Thickness	Shell Electron Density (e^-/nm^3)
$9.3^{+0.25}_{-0.20}$	0	2900

Figure S6.1. 0 % Au nanoparticle sample SAXS spectrum and fitting model. SAXS data was collected and the form factor fit in order to determine relevant morphological parameters, which are included in the table below the plot. In this case the electron density of the particle was fixed to that of bulk Ag.

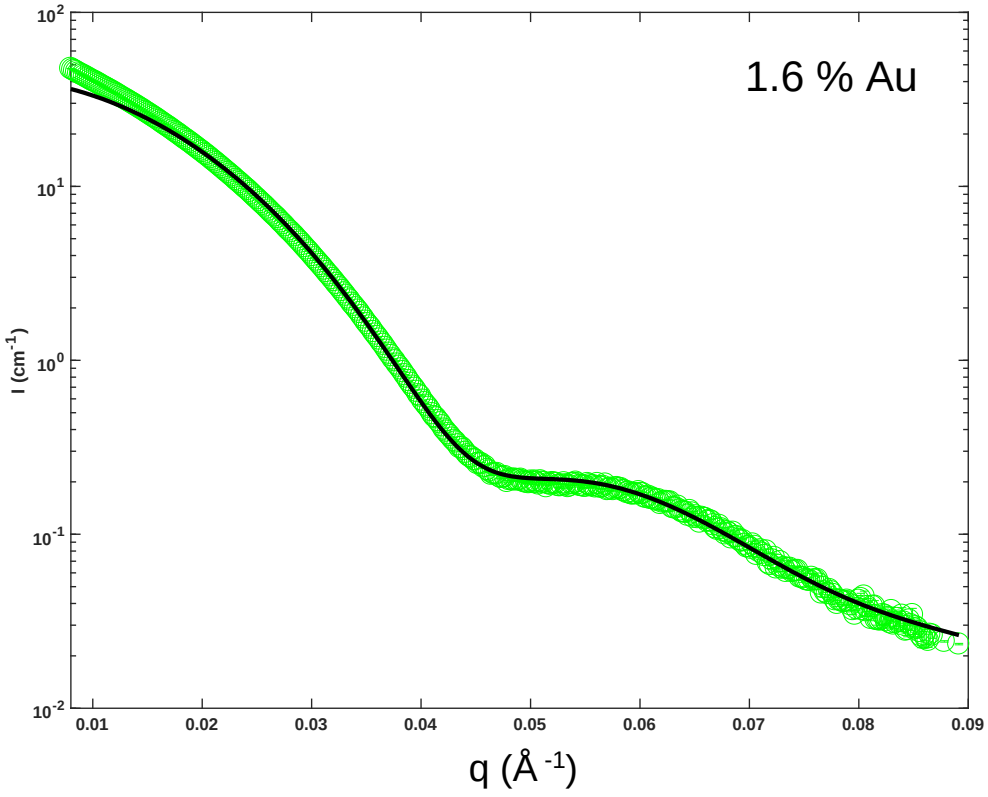

Total Particle Radius (nm)	Core Radius:Shell Thickness	Shell Electron Density (e^-/nm^3)
$9.3^{+0.6}_{-0.1}$	$0.150^{+0.004}_{-0.004}$	2921

Figure S6.2. 1.6 % Au nanoparticle sample SAXS spectrum and fitting model. SAXS data was collected and the form factor fit in order to determine relevant morphological parameters, which are included in the table below the plot.

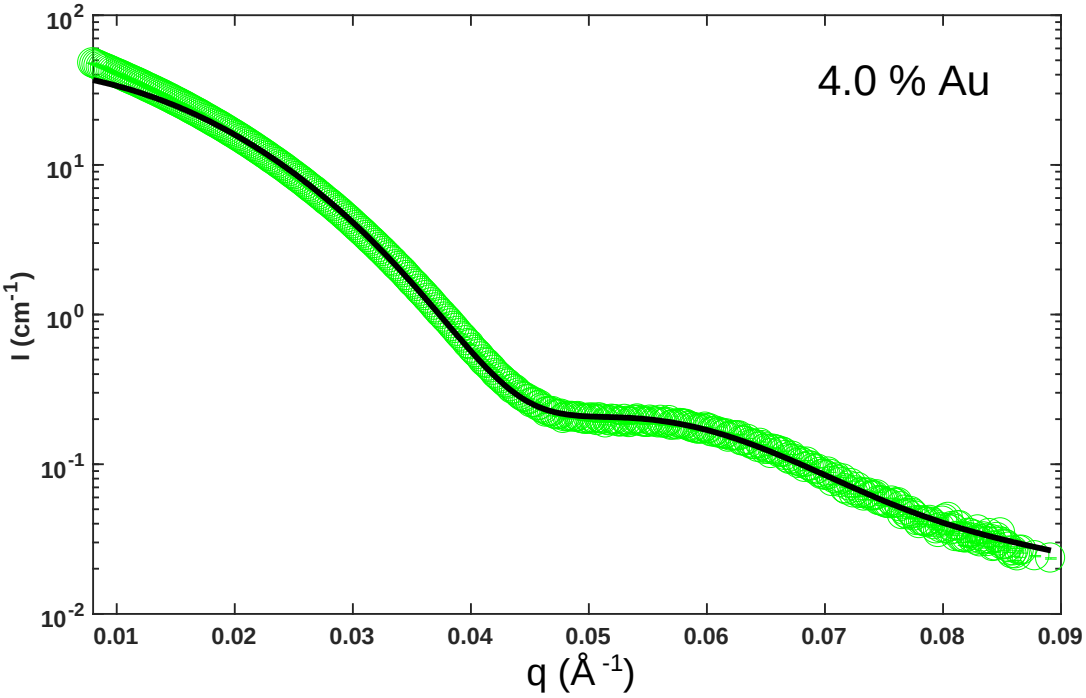

Total Particle Radius (nm)	Core Radius:Shell Thickness	Shell Electron Density (e^-/nm^3)
$9.3^{+0.7}_{-0.1}$	$0.150^{+0.003}_{-0.003}$	2920

Figure S6.3. 4.0 % Au nanoparticle sample SAXS spectrum and fitting model. SAXS data was collected and the form factor fit in order to determine relevant morphological parameters, which are included in the table below the plot.

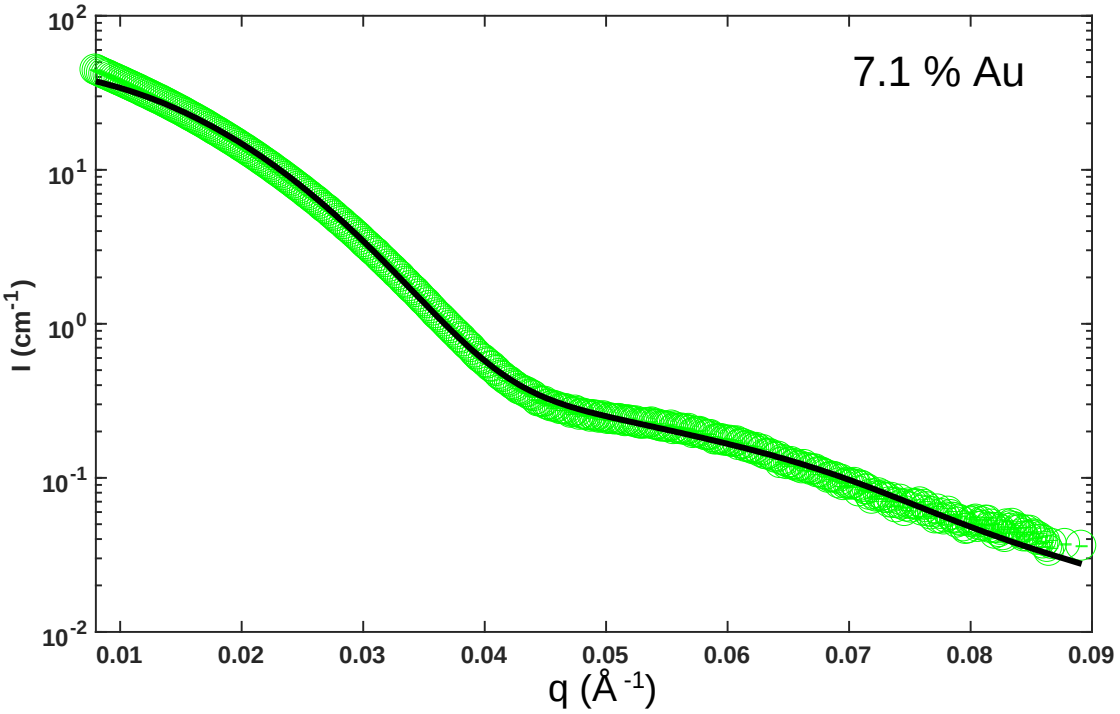

Total Particle Radius (nm)	Core Radius:Shell Thickness	Shell Electron Density (e^-/nm^3)
$9.4^{+0.3}_{-0.1}$	$0.191^{+0.005}_{-0.005}$	2919

Figure S6.4. 7.1 % Au nanoparticle sample SAXS spectrum and fitting model. SAXS data was collected and the form factor fit in order to determine relevant morphological parameters, which are included in the table below the plot.

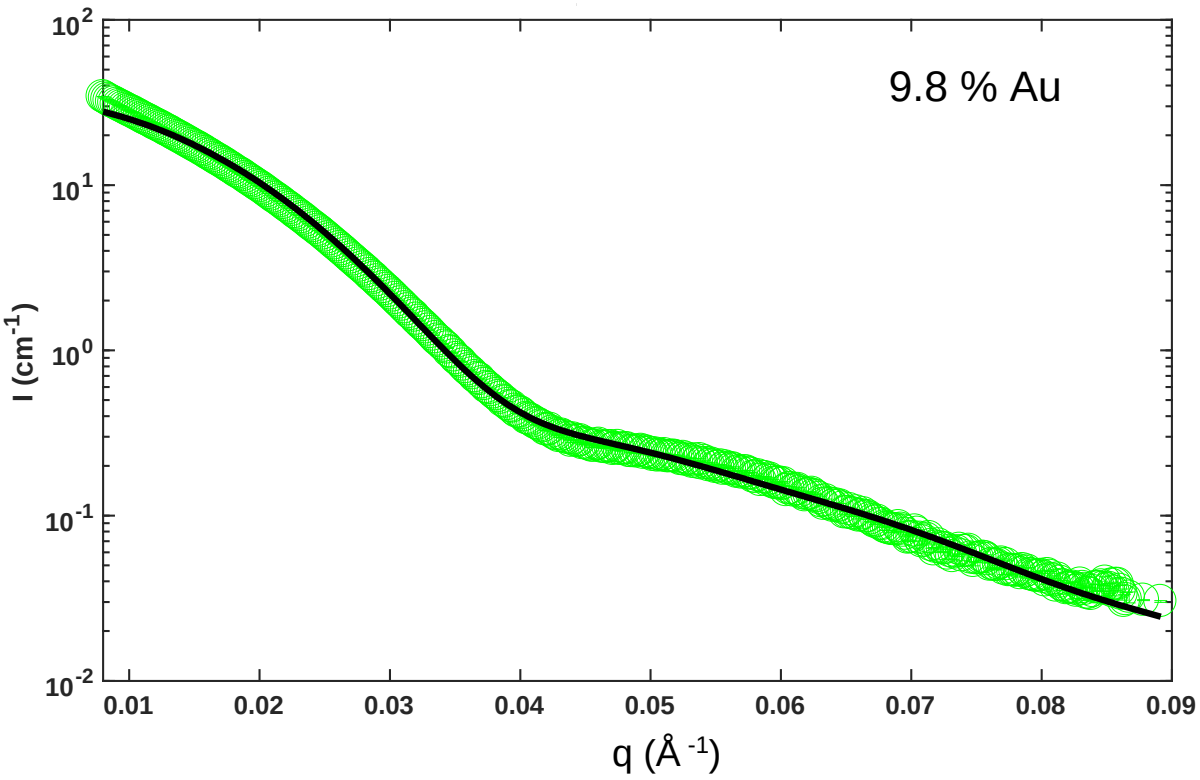

Total Particle Radius (nm)	Core Radius:Shell Thickness	Shell Electron Density (e^-/nm^3)
$9.5^{+0.3}_{-0.3}$	$0.346^{+0.008}_{-0.008}$	2905

Figure S6.5. 9.8 % Au nanoparticle sample SAXS spectrum and fitting model. SAXS data was collected and the form factor fit in order to determine relevant morphological parameters, which are included in the table below the plot.

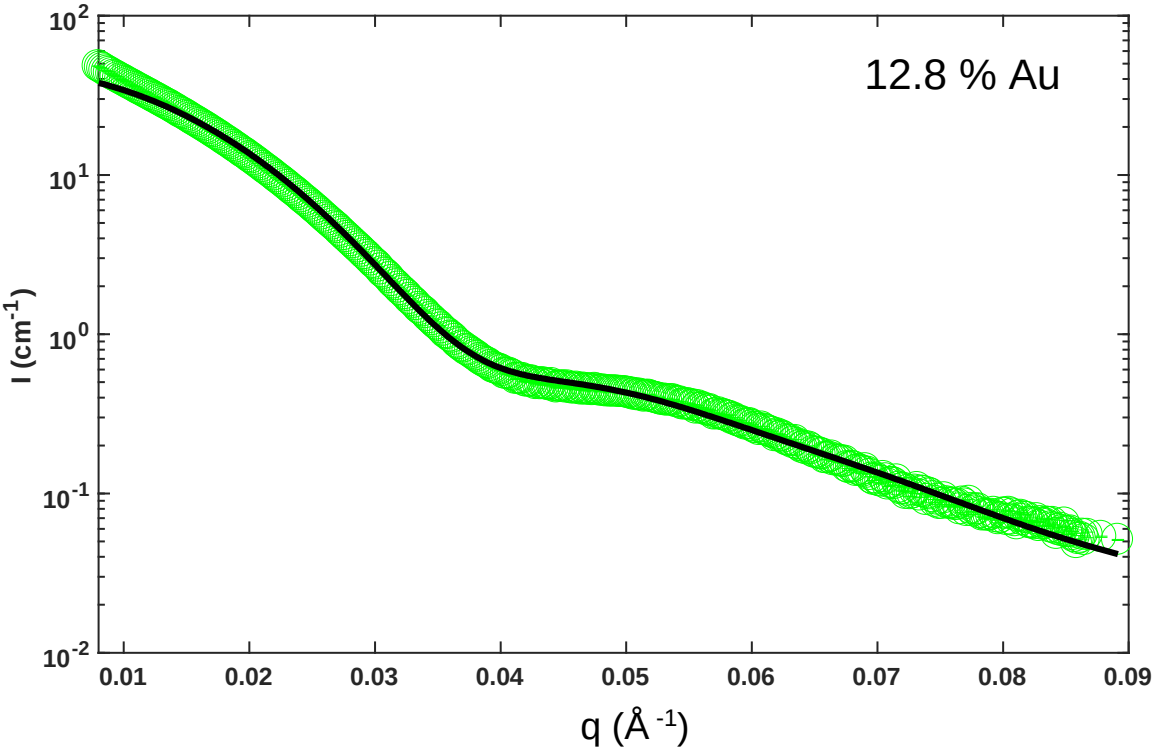

Total Particle Radius (nm)	Core Radius:Shell Thickness	Shell Electron Density (e^-/nm^3)
$9.5^{+0.3}_{-0.3}$	$0.49^{+0.01}_{-0.04}$	2921

Figure S6.6. 12.8 % Au nanoparticle sample SAXS spectrum and fitting model. SAXS data was collected and the form factor fit in order to determine relevant morphological parameters, which are included in the table below the plot.

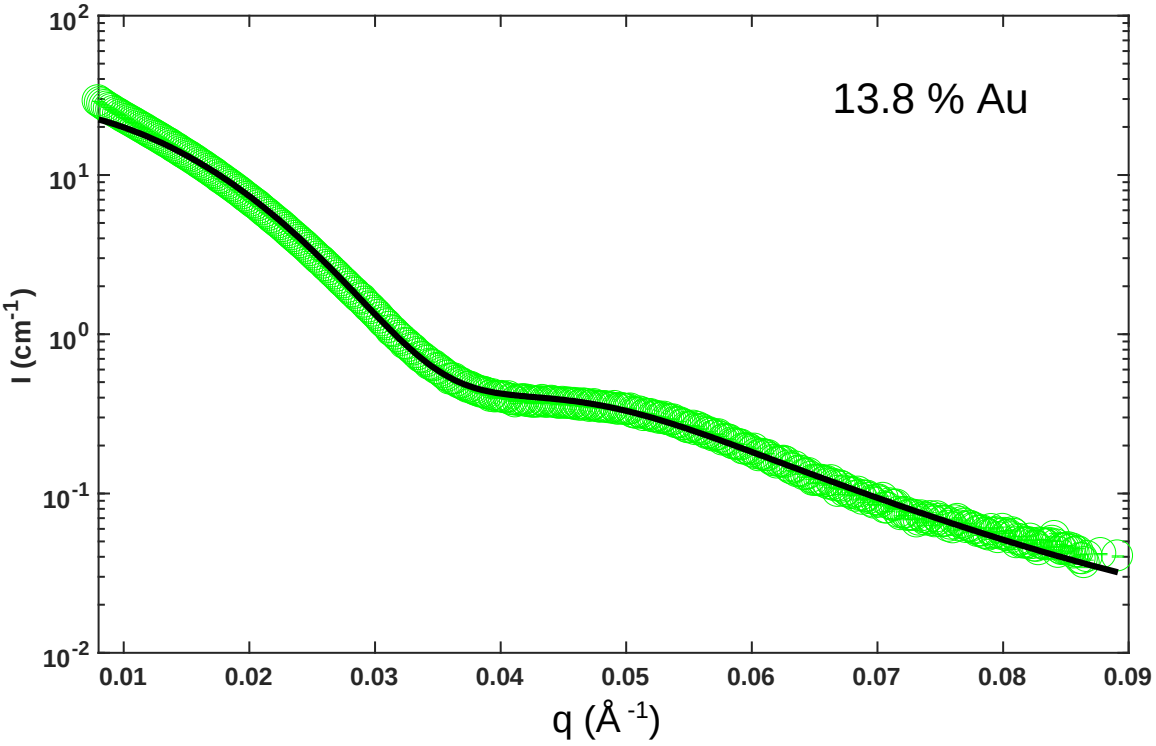

Total Particle Radius (nm)	Core Radius:Shell Thickness	Shell Electron Density (e^-/nm^3)
$9.6^{+0.4}_{-0.3}$	$0.67^{+0.02}_{-0.02}$	2902

Figure S6.7. 13.8 % Au nanoparticle sample SAXS spectrum and fitting model. SAXS data was collected and the form factor fit in order to determine relevant morphological parameters, which are included in the table below the plot.

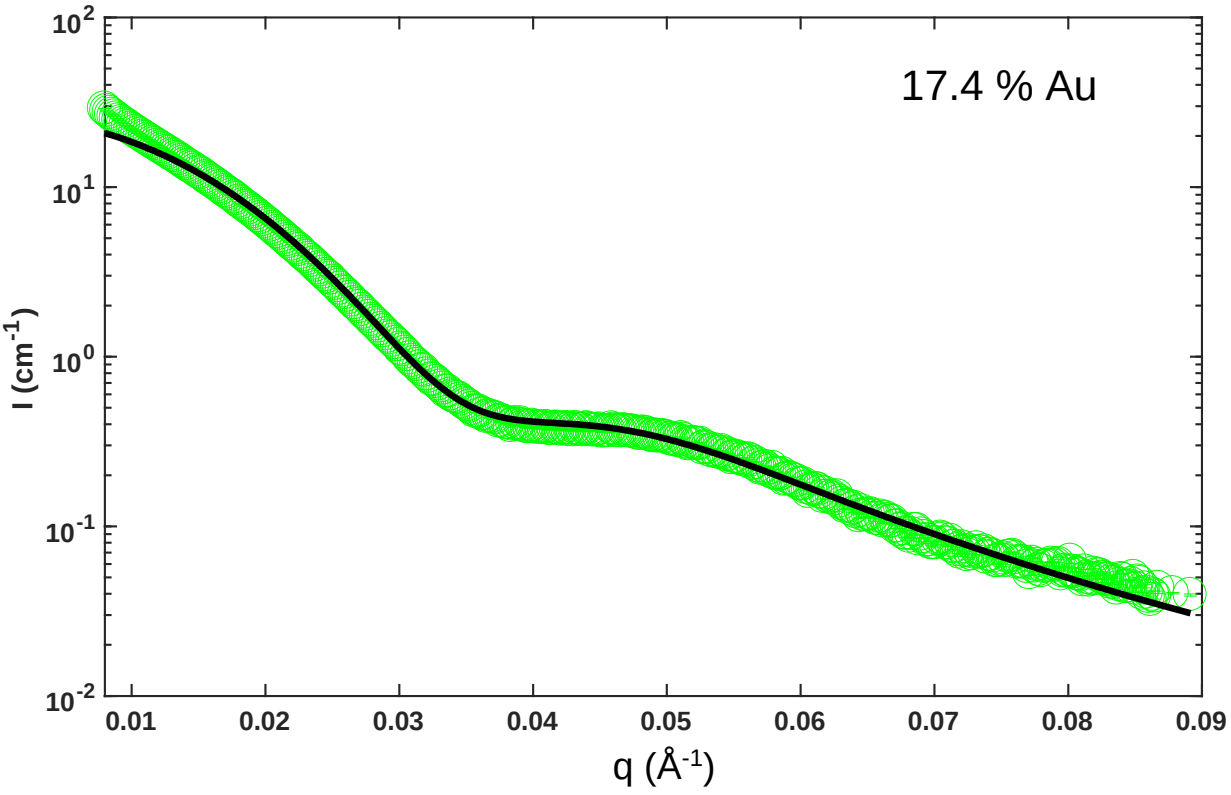

Total Particle Radius (nm)	Core Radius:Shell Thickness	Shell Electron Density (e^-/nm^3)
$9.9^{+0.4}_{-0.4}$	$0.73^{+0.02}_{-0.02}$	2904

Figure S6.8. 17.4 % Au nanoparticle sample SAXS spectrum and fitting model. SAXS data was collected and the form factor fit in order to determine relevant morphological parameters, which are included in the table below the plot.

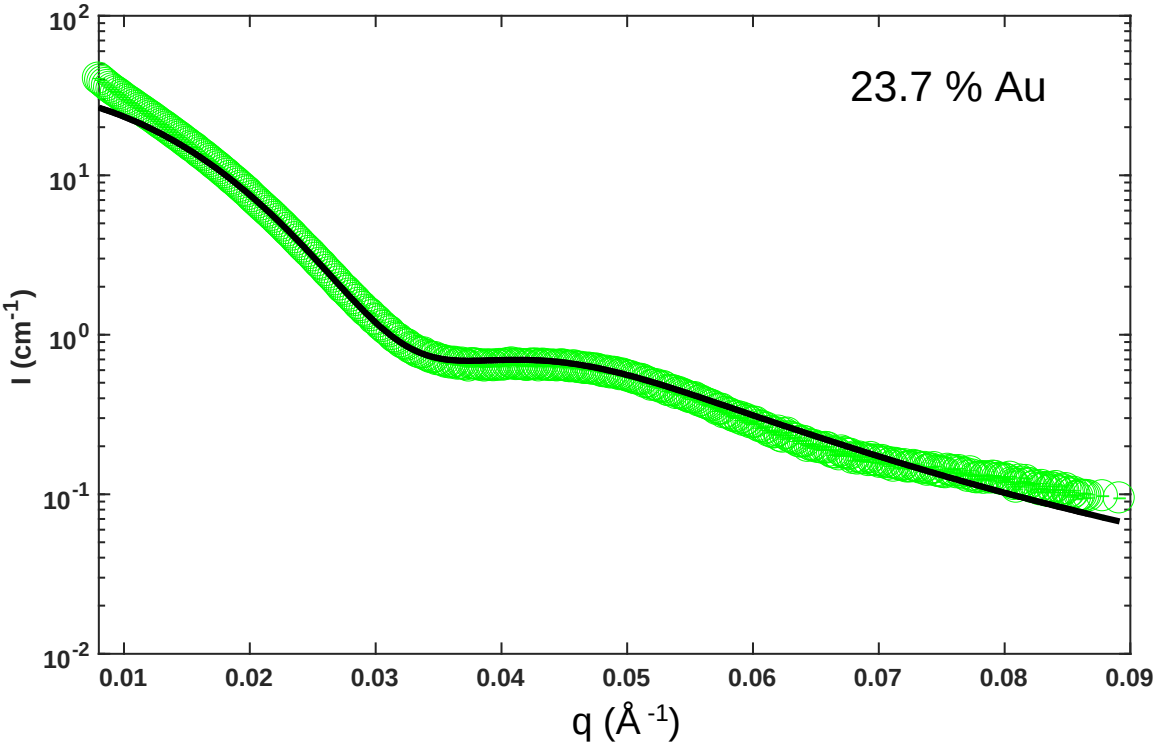

Total Particle Radius (nm)	Core Radius:Shell Thickness	Shell Electron Density (e^-/nm^3)
$10.2^{+0.5}_{-0.5}$	$0.83^{+0.08}_{-0.02}$	2919

Figure S6.9. 23.7 % Au nanoparticle sample SAXS spectrum and fitting model. SAXS data was collected and the form factor fit in order to determine relevant morphological parameters, which are included in the table below the plot.

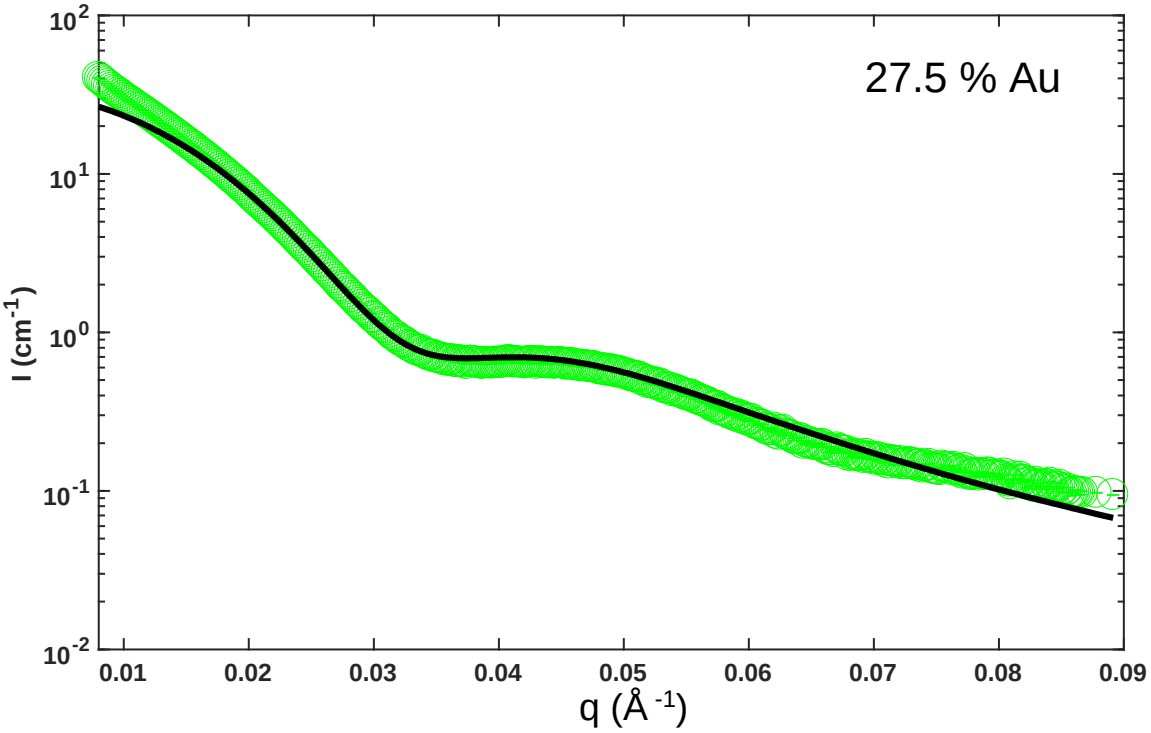

Total Particle Radius (nm)	Core Radius:Shell Thickness	Shell Electron Density (e^-/nm^3)
$10.4^{+0.5}_{-0.5}$	$0.89^{+0.02}_{-0.02}$	2916

Figure S6.10. 27.5 % Au nanoparticle sample SAXS spectrum and fitting model. SAXS data was collected and the form factor fit in order to determine relevant morphological parameters, which are included in the table below the plot.

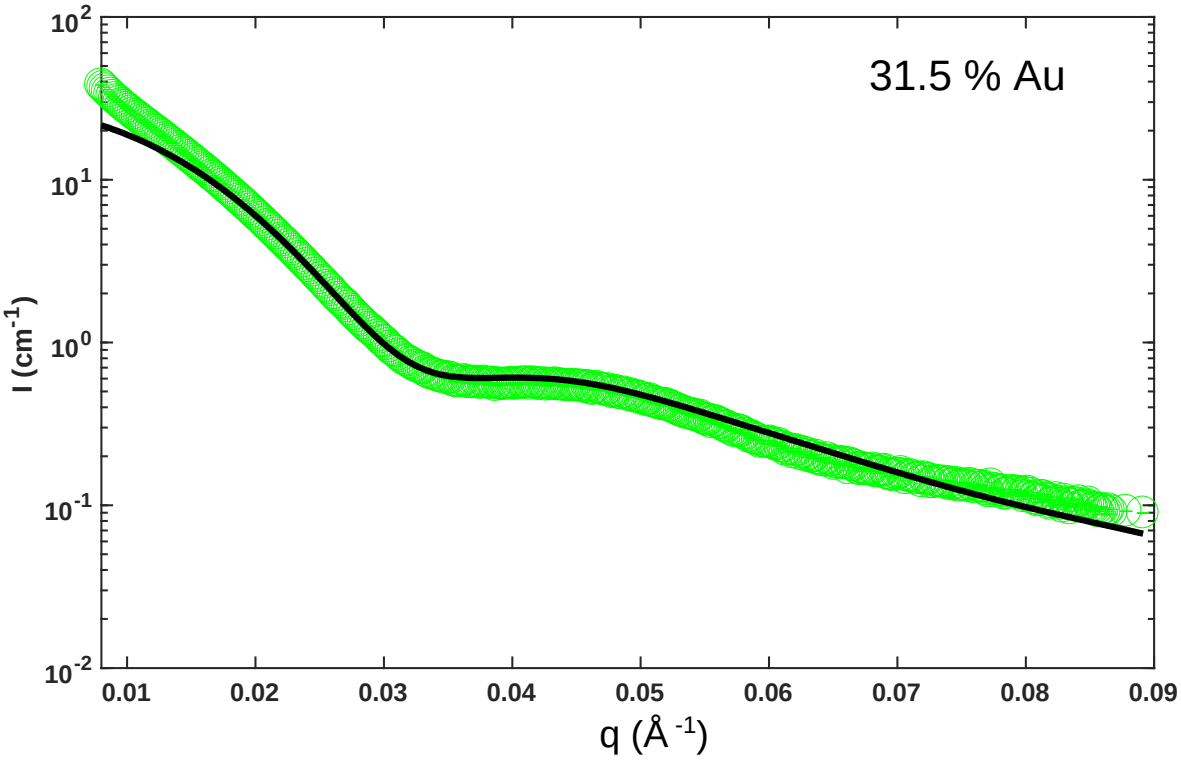

Total Particle Radius (nm)	Core Radius:Shell Thickness	Shell Electron Density (e^-/nm^3)
$10.5^{+0.6}_{-0.4}$	$0.90^{+0.09}_{-0.02}$	2945

Figure S6.11. 31.5 % Au nanoparticle sample SAXS spectrum and fitting model. SAXS data was collected and the form factor fit in order to determine relevant morphological parameters, which are included in the table below the plot.

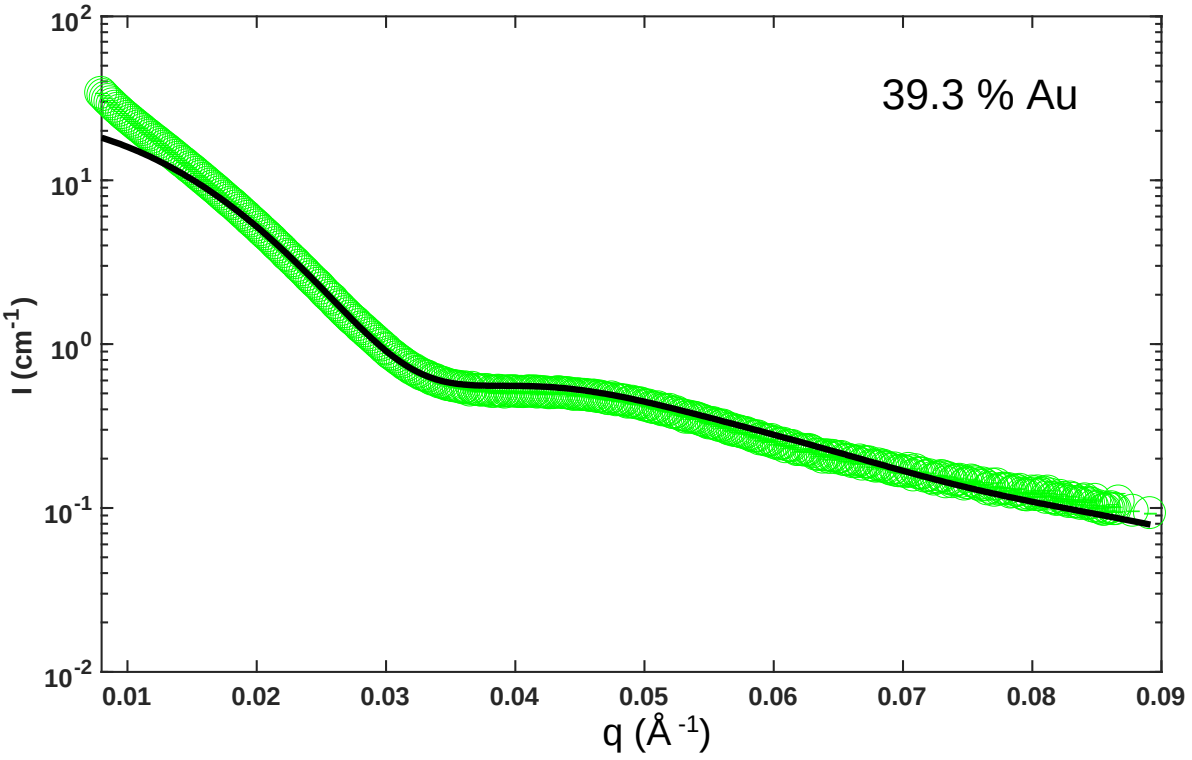

Total Particle Radius (nm)	Core Radius:Shell Thickness	Shell Electron Density (e^-/nm^3)
$10.3^{+0.5}_{-0.4}$	$0.97^{+0.02}_{-0.02}$	2899

Figure S6.12. 39.3 % Au nanoparticle sample SAXS spectrum and fitting model. SAXS data was collected and the form factor fit in order to determine relevant morphological parameters, which are included in the table below the plot.

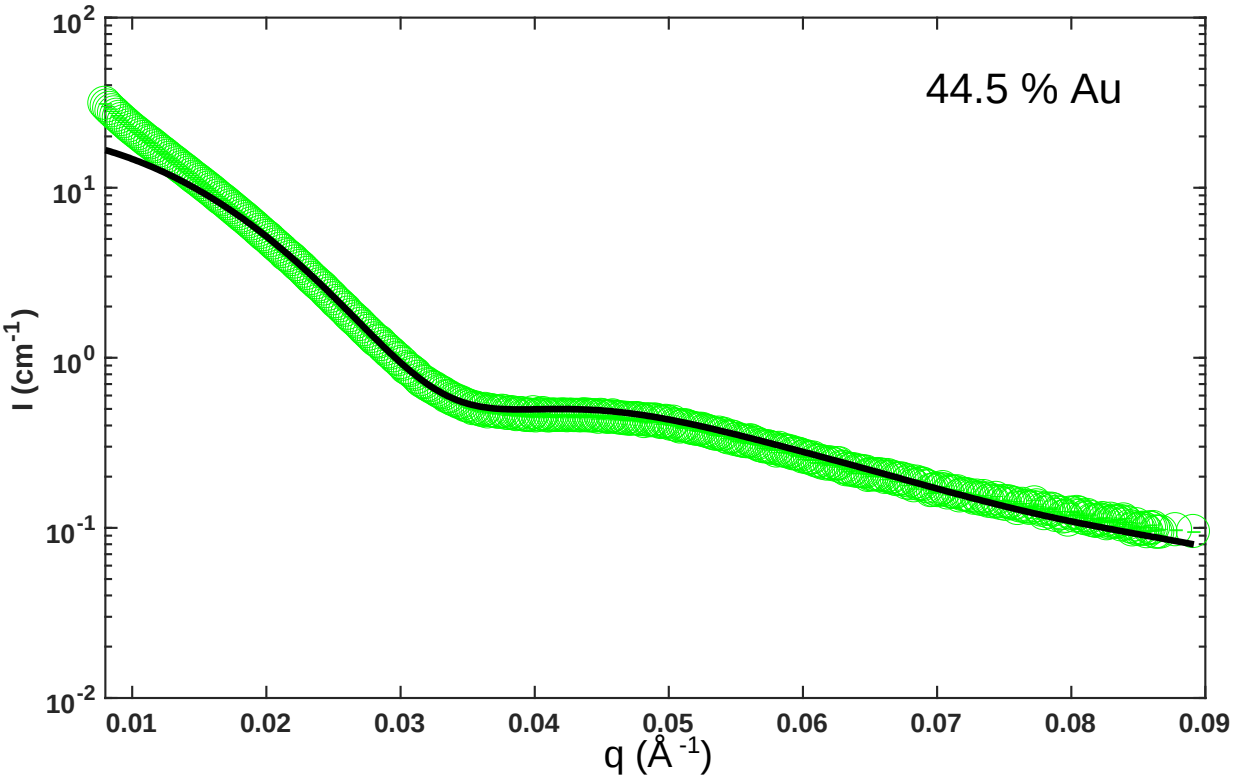

Total Particle Radius (nm)	Core Radius:Shell Thickness	Shell Electron Density (e^-/nm^3)
$10.0^{+0.4}_{-0.4}$	$0.99^{+0.03}_{-0.03}$	2896

Figure S6.13. 44.5 % Au nanoparticle sample SAXS spectrum and fitting model. SAXS data was collected and the form factor fit in order to determine relevant morphological parameters, which are included in the table below the plot.

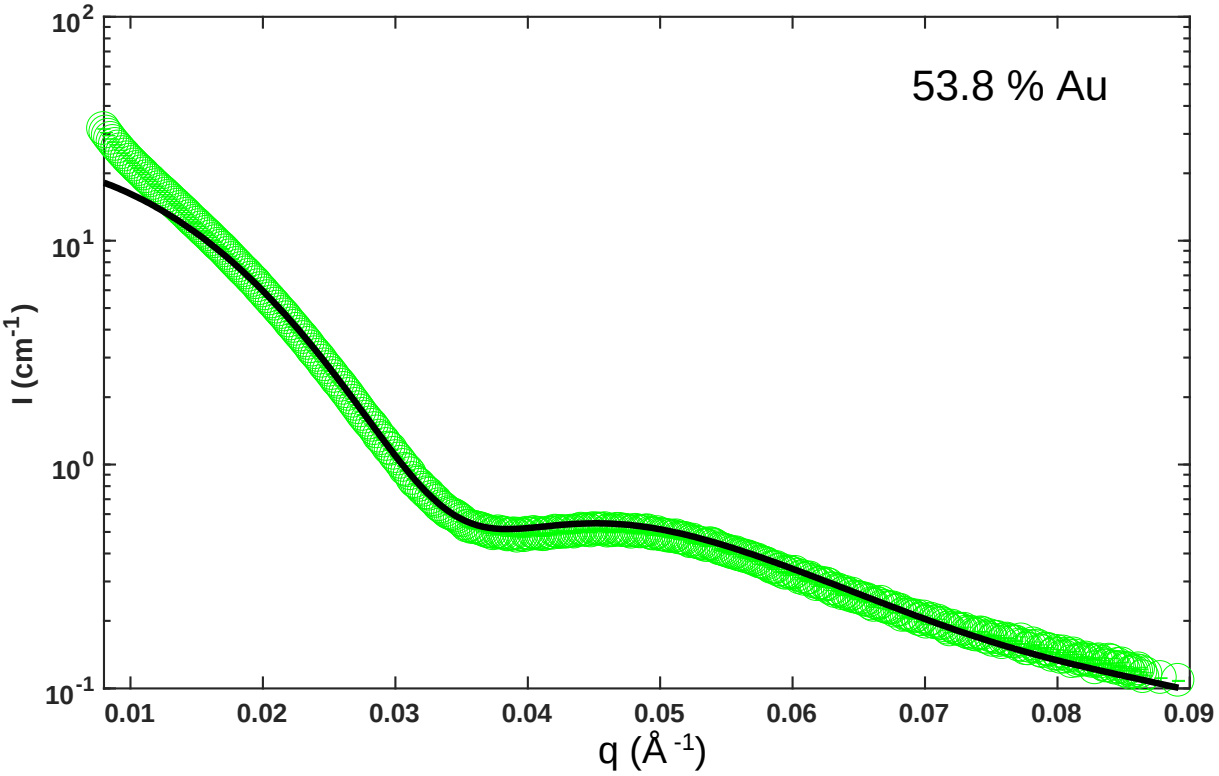

Total Particle Radius (nm)	Core Radius:Shell Thickness	Shell Electron Density (e^-/nm^3)
$9.8^{+0.3}_{-0.4}$	$1.09^{+0.02}_{-0.03}$	2882

Figure S6.14. 53.8 % Au nanoparticle sample SAXS spectrum and fitting model. SAXS data was collected and the form factor fit in order to determine relevant morphological parameters, which are included in the table below the plot.

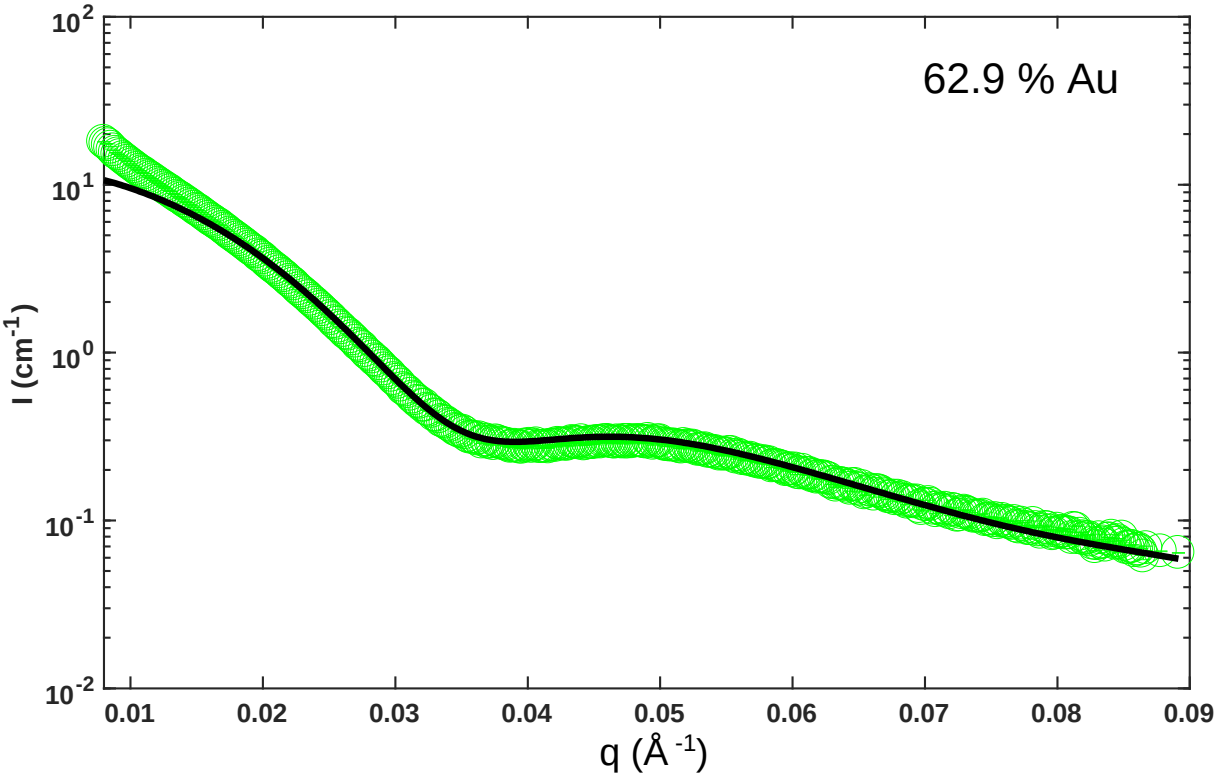

Total Particle Radius (nm)	Core Radius:Shell Thickness	Shell Electron Density (e^-/nm^3)
$9.6^{+0.4}_{-0.4}$	$1.10^{+0.02}_{-0.03}$	2931

Figure S6.15. 62.9 % Au nanoparticle sample SAXS spectrum and fitting model. SAXS data was collected and the form factor fit in order to determine relevant morphological parameters, which are included in the table below the plot.

Multi-Shell SAXS Data + Fits

The measured intensity profile *I*(*q*) could be reasonably described by assuming a spherical core-shell model. Due to irregularity in shape and deviation from the used single-shell model, another analytical model was used to attempt to minimize the error in using the core-shell model. The transformed nanoparticles, as seen in the electron micrographs (Fig 3), can be thought of has having a diffuse outer layer created by protrusions that extend beyond the average outer shell radius. By appending a third layer to the core-shell model we have attempted to contain the additional, small but excess, electron density with a low density shell that was allowed to freely range in size

during the fitting process. Results from this model were similar to the original single-shell model with an extended average total size. This model also tracked the electron density of both the primary and secondary shells and showed that consistently the inner shell contained the majority of the electron density of the particle, despite allowing the outer shell to extend to a maximum of 30 nm during fitting. This leads to the conclusion that the outer shell is extremely diffuse and contains very little actual mass using this model. The comparison between the results of the single-shell and multi-shell model fits are negligible and the confidence intervals on the individual tracked parameters are narrower in the single-shell model presented in the main text.

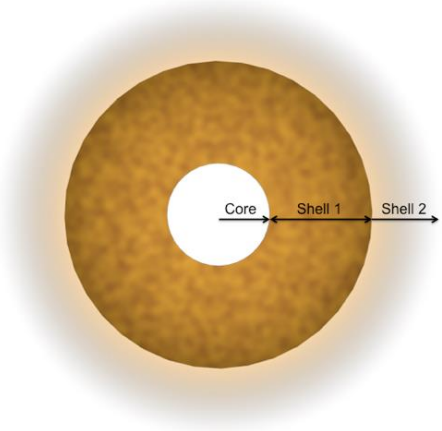

Figure S7. Pictorial schematic of multi-shell SAXS model. A better low-q fit was obtained for the SAXS data through use of a more complex model. This model involves an additional diffuse shell outside of the first dense shell. This may be due to the rough surface layers of the nanoparticle subsequent to exchange, resulting in a quasi-spherical particle.

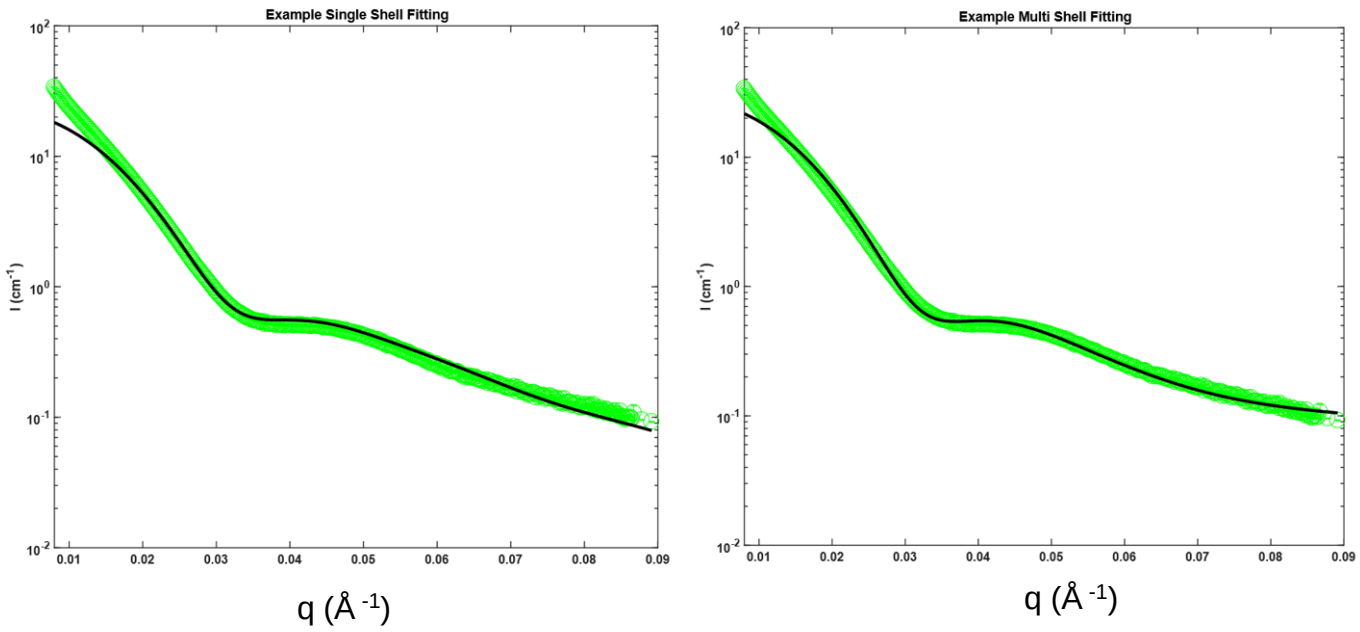

Figure S8. Example of single vs. multi-shell SAXS models. The same SAXS data (39.3 % Au) fit with two different models (single-shell, left, and multi-shell, right), shows good agreement for both models. Yet the multi-shell model shows an improvement in the goodness-of-fit in the low-q region.

Figure S8 (above) shows the fits (red) of the same X-Ray Scattering spectrum (black, 39.3 % Au). The multi-shell fit (right) provides a better fit for the spectra at low values of q. This is likely only due to the fact that the model includes more parameters within the fit and is mathematically more flexible. The parameters tracked include: total mean radius, core to shell thickness ratio, second shell thickness, shell 1 and shell 2 density and polydispersity.

However, introduction of additional parameters increases the error associated with the individual parameter. The mutli-shell model contains 6 independent parameters, while the single-shell model only includes 4, thus introducing unneeded error into the relevant parameters for examining the relevant mechanism. Comparison of these features between the two models reveals a similar trend of approximately the same values with exaggerated error in the multi-shell model (Figure S9 below).

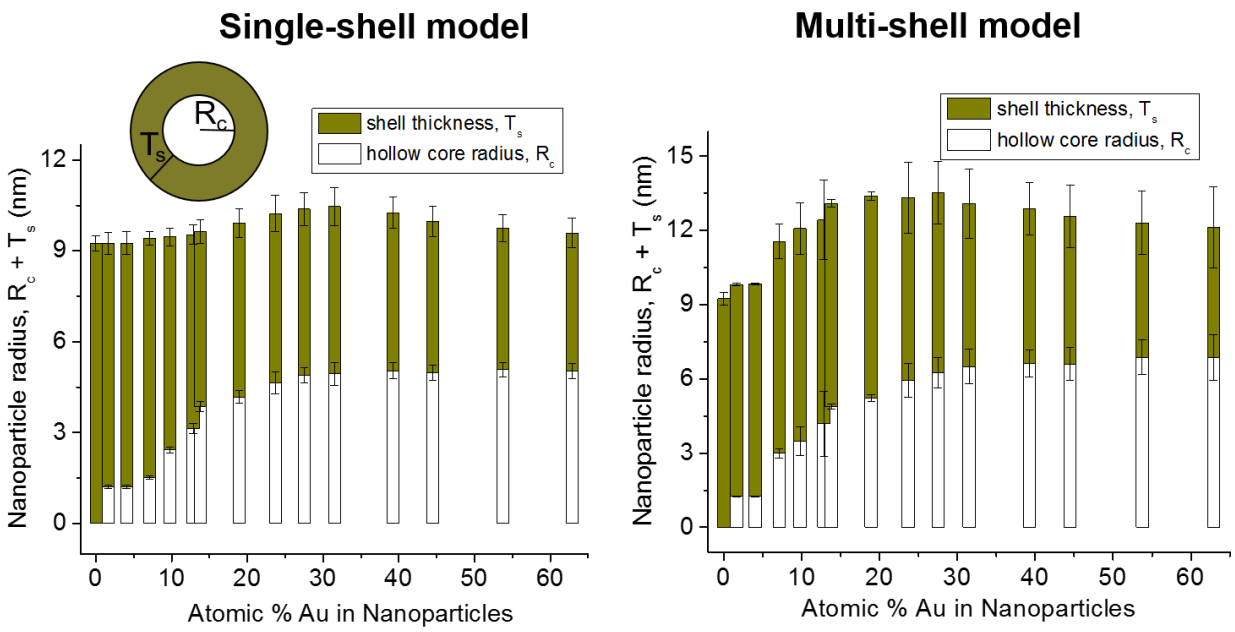

Figure S9. Parameter comparison between single and multi-shell SAXS models. While overall nanoparticle radius is slightly larger in the multi-shell case due to the inclusion of a secondary diffuse shell, parameter trends of hollow core growth along with decreasing shell thickness are consistent between the two separate models, demonstrating the repeatability of these trends.

Nanoparticle Size Determination

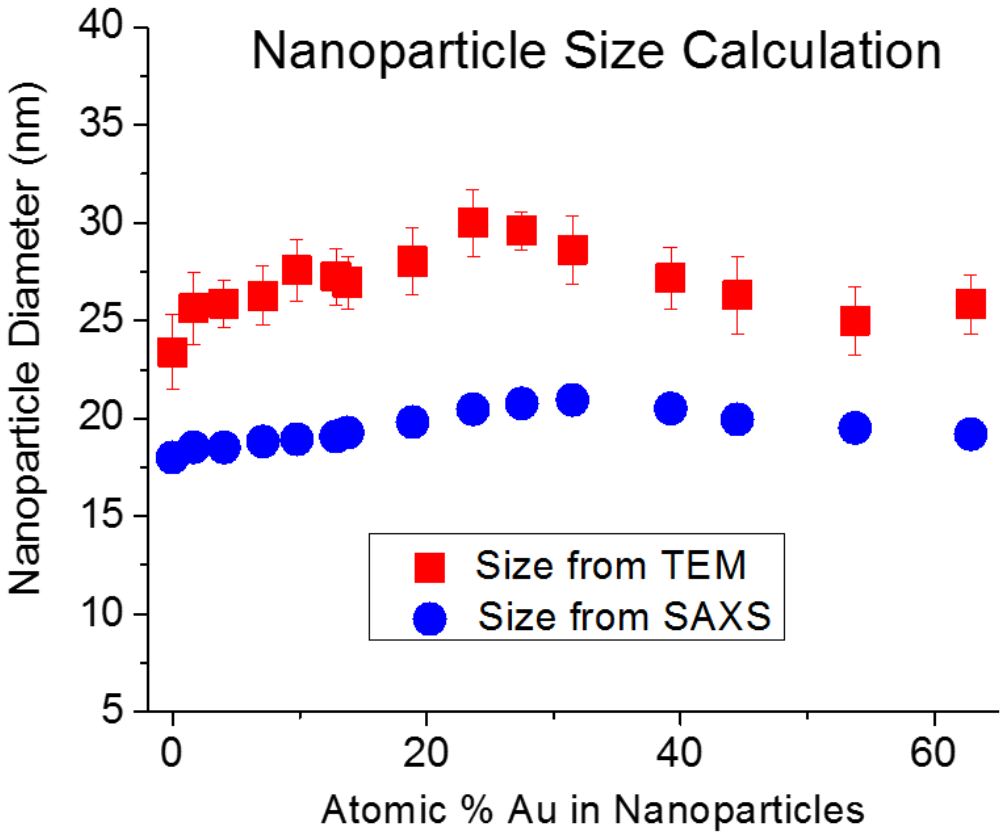

Figure S10. Nanoparticle Size Determination. Nanoparticle size as a function of Au atomic % within the nanoparticles is plotted as determined from TEM size analysis and SAXS form factor modeling. While slightly smaller nanoparticle sizes were determined from SAXS modeling, the trend persists that the nanoparticle size is not highly variant throughout the Galvanic replacement reaction.

XANES Results

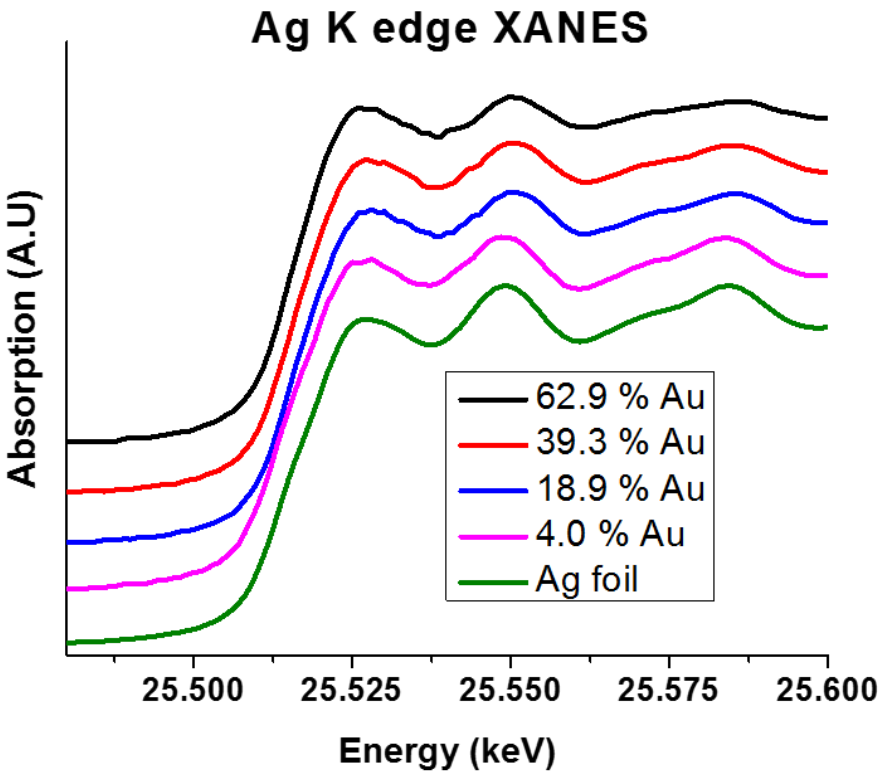

Figure S11. Ag K edge XANES spectra. Ag XANES spectra of each of the nanoparticle samples, regardless of transformation stage or Au content, resemble that of an Ag foil (green). This shows that Ag is in the Ag^0 state.

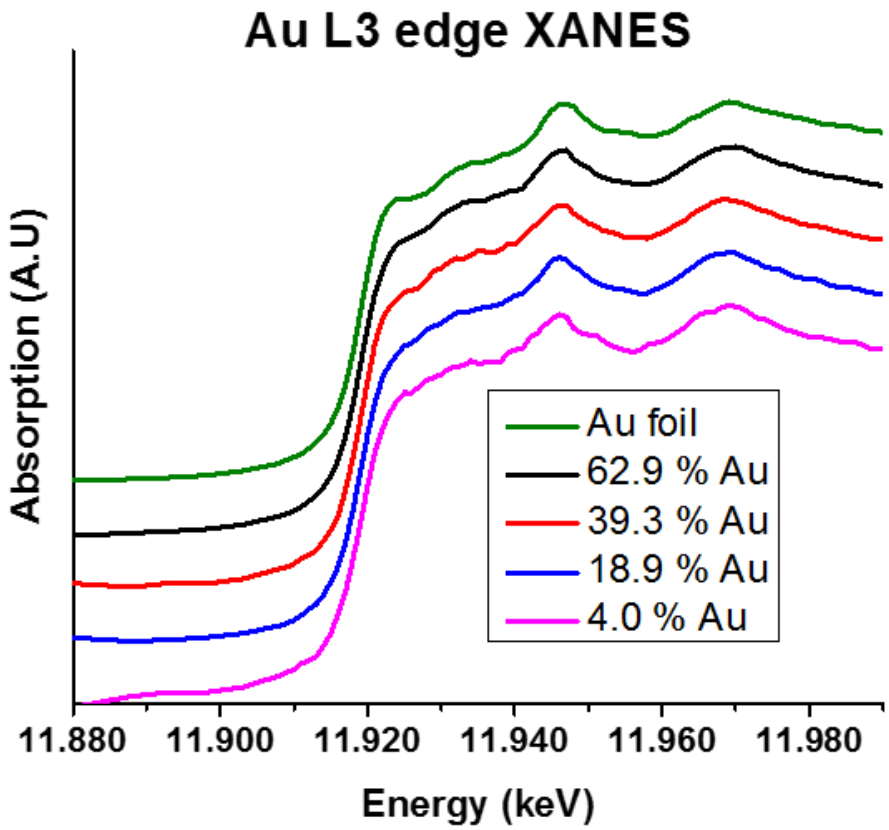

Figure S12. Au L3 edge XANES spectra. Au XANES spectra of each of the nanoparticle samples resemble the Au foil pattern (green) in both the edge and near-edge regions. This suggests that Au is in a similar reduced state (Au^0).

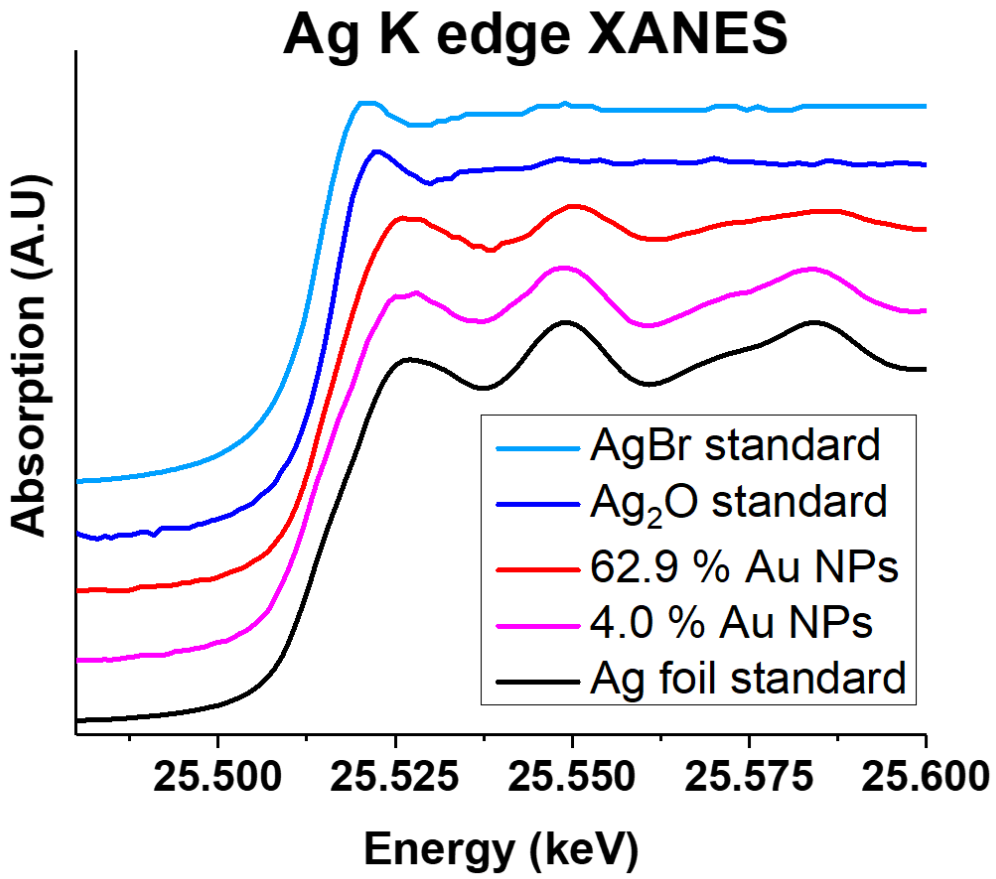

Figure S13. Comparison of Ag K edge XANES spectra. We compare nanoparticle spectra from low (magenta) and high (red) Au atomic % stages in the transformation from Ag nanospheres to AgAu nanocages to Ag^0 and Ag^+ standards. In order to investigate the possible prescence of An Ag^+ species from Cl^- or O^{2-} etching, we compare the NP spectra to AgO_2 and AgBr (which should have a similar density of states to AgCl) standards, and find that both NP spectra more closely resemble the Ag foil standard (Ag^0). This reveals that the Ag within the particles is Ag^0.

XAFS Spectra and Fitting Models

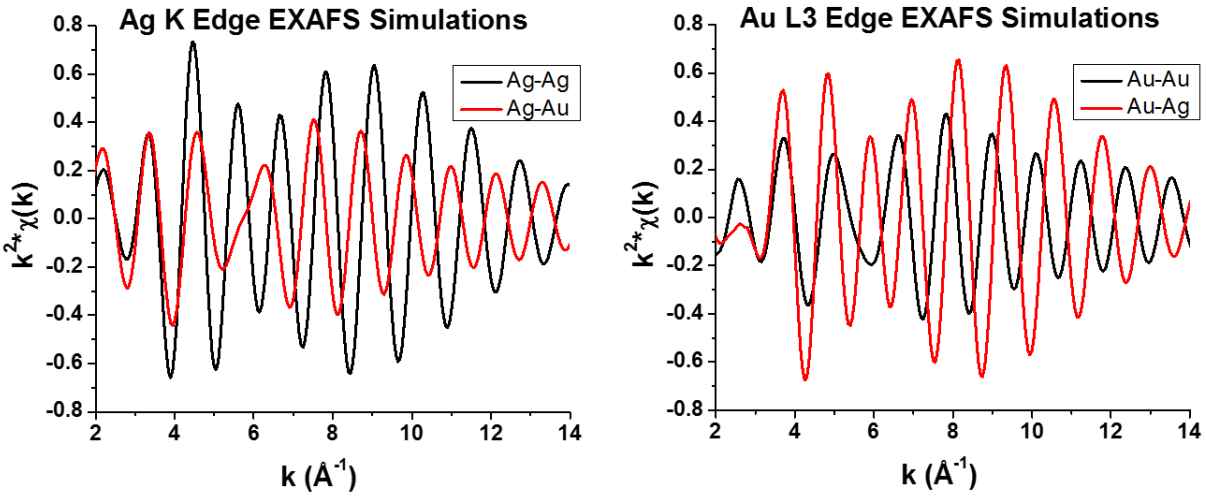

Figure S14. Ag K edge and Au L3 edge simulations show we can distinguish Ag-Ag and Ag-Au as well as Au-Au and Au-Ag pathways. Ag K edge simulations (left) and Au L3 edge simulations (right) of first shell pathways set at 2.884 Å with all identical parameters (coordination number, σ^2, etc.) are shown. Changes in phase shift result in an offset in the phase of the scattering pathways. There is also a notable difference in the scattering amplitude as a function of k. These drastic spectral differences enable quantitative analysis of the amounts of Ag-Ag, Ag-Au and Au-Au present within the nanoparticles as a function of their transformation.

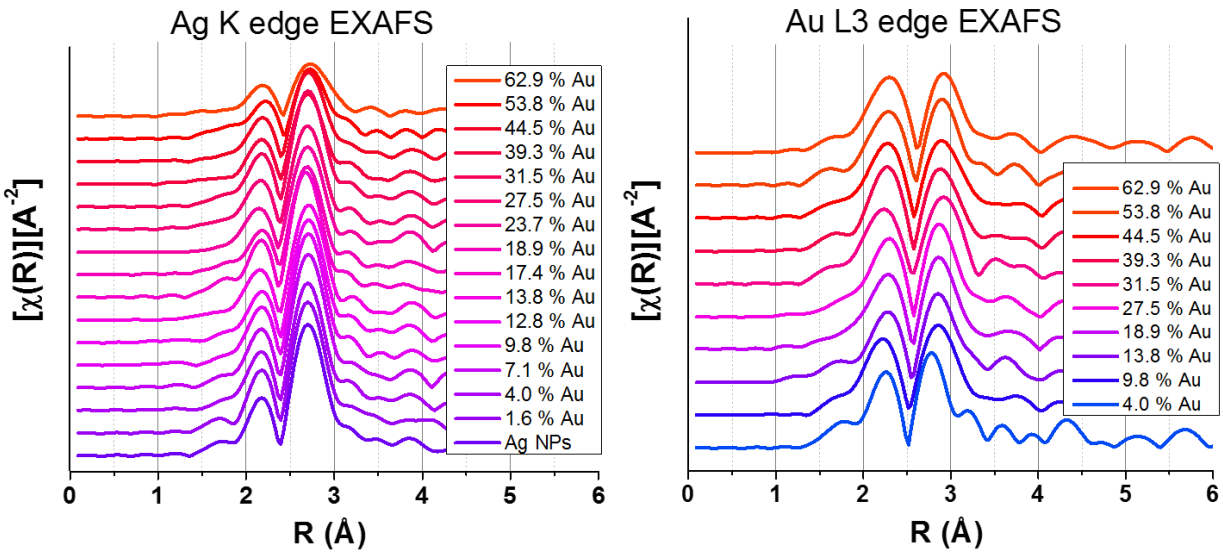

Figure S15. Ag K edge and Au L3 edge EXAFS data as a function of nanoparticle transformation. Ag K edge EXAFS spectra (left) and Au L3 edge EXAFS spectra (right) are plotted with vertical offsets in a gradient from low-Au content (blue) to high-Au content (red). The spectral features remain relatively constant throughout due to the high concentration of Ag-Ag and Au-Au bonds as a result of local phase segregation.

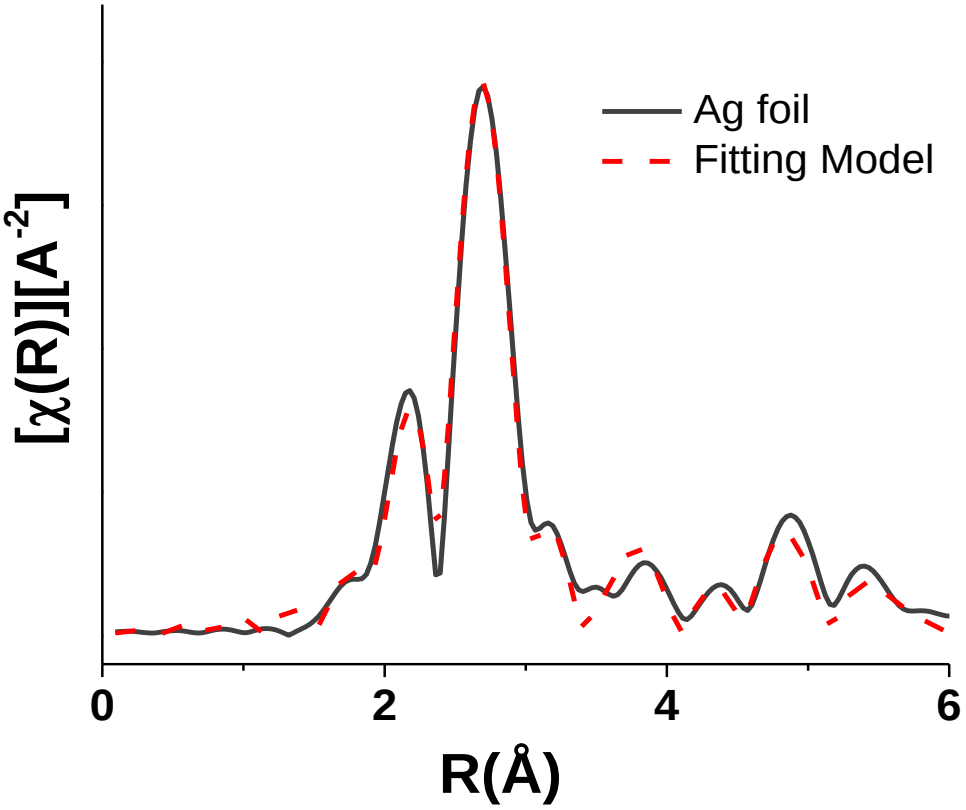

Pathway	N_{theory}	S_0^2	R (Å)	E_0 (eV)	σ^2 (Å^2) x 10^{-3}
Ag–Ag (shell 1)	12	0.74	2.866	2.35	8.03
Ag–Ag (shell 2)	6	0.74	4.062	2.35	9.85
Ag–Ag (shell 3)	24	0.74	5.009	2.35	12.1

Figure S16.1. Ag foil EXAFS standard and fitting model. Ag foil data was collected and modeled in order to determine the amplitude reduction factor (S_0^2), since the coordination number is a fixed known. A fitting range from 1.5 to 5 Å and a k-range from 2 to 12 Å^{-1} was used. The R-factor parameter associated with the goodness of fit for this model was 0.034.

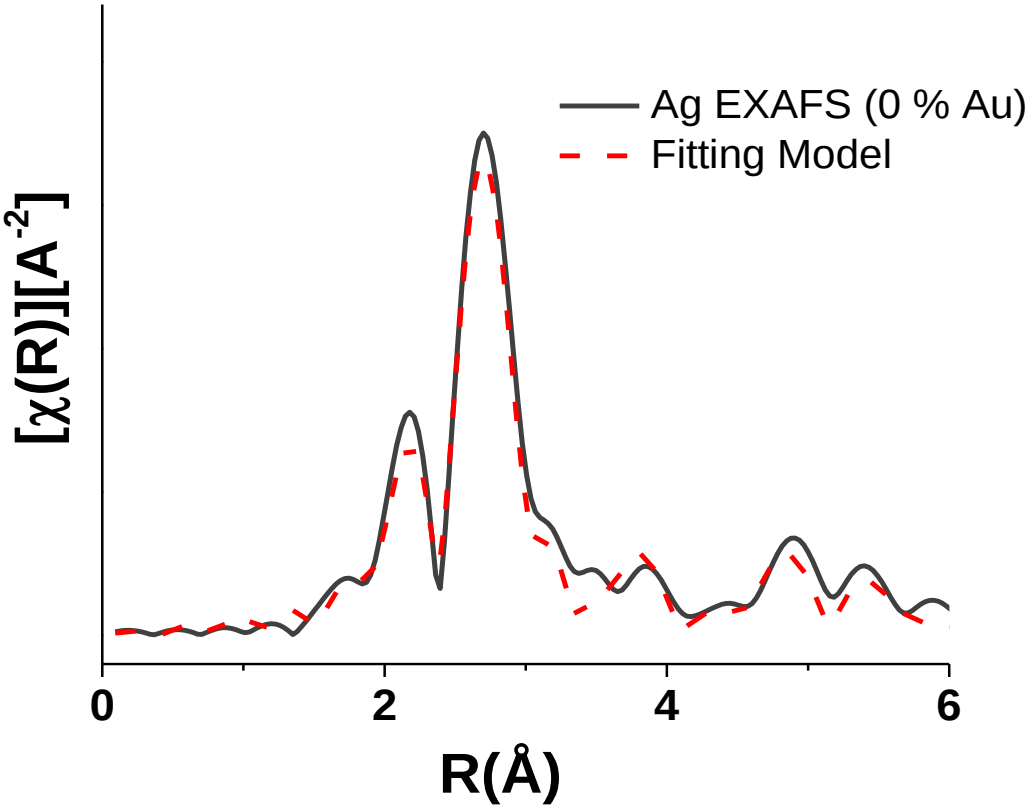

Pathway	N	R (Å)	E_0 (eV)	σ^2 (Å^2) x 10^{-3}
Ag–Ag (shell 1)	11.9 ± 0.8	2.862 ± 0.004	3.4 ± 0.3	9.3 ± 0.5

Figure S16.2. Starting template Ag nanoparticle EXAFS spectrum and fitting model. The Ag K-edge nanoparticle spectrum was fit using first coordination-shell Ag atomic pathways. A fitting range from 1.5 to 3.5 Å and a k-range from 2 to 12 Å^{-1} was used. The R-factor parameter associated with the goodness of fit for this model was 0.023.

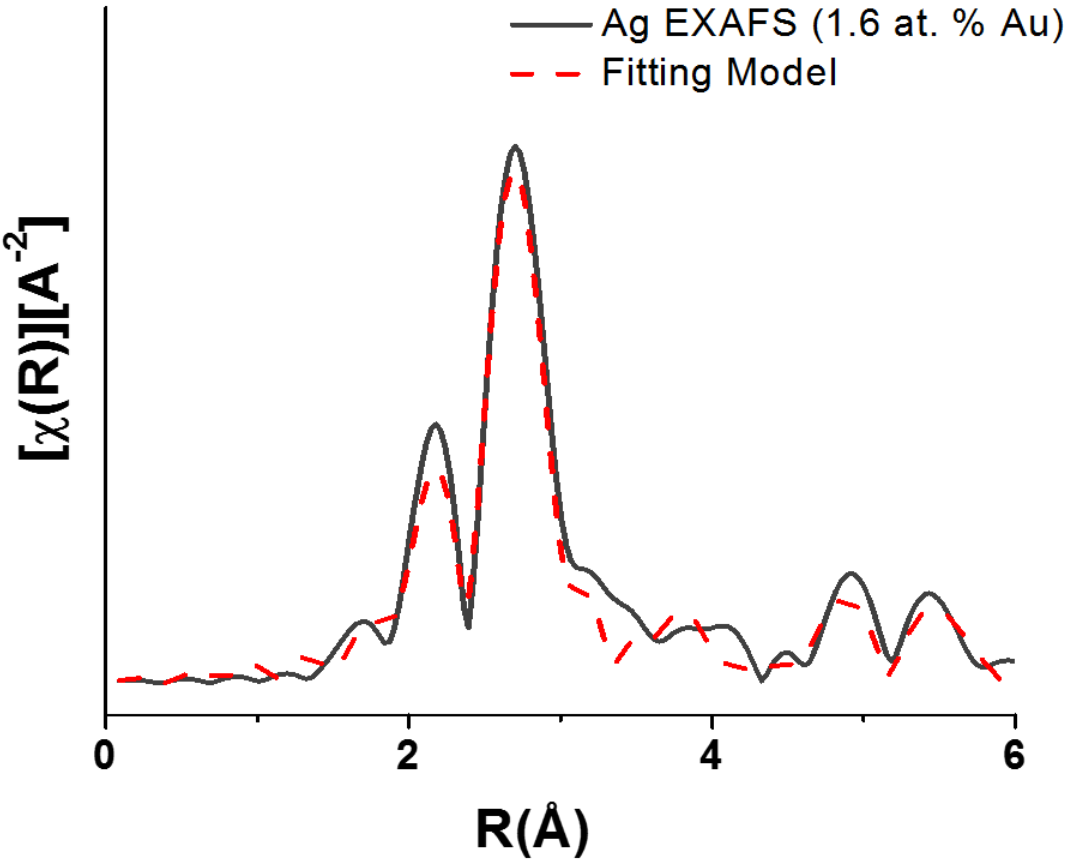

Pathway	N	R (Å)	E_0 (eV)	σ^2 (Å^2) x 10^{-3}
Ag–Ag (shell 1)	11.9 ± 1.6	2.861 ± 0.008	3.3 ± 1.2	9.0 ± 0.9
Ag–Au (shell 1)	0.5 ± 0.5	2.89 ± 0.09	2.4 ± 3.2	7.9 ± 6.3

Figure S16.3. Ag K edge EXAFS spectrum and fitting model for 1.6 at. % Au nanoparticle sample. The Ag K-edge nanoparticle spectrum was fit using first coordination-shell atomic pathways. A fitting range from 1.5 to 3.5 Å and a k-range from 2 to 12 Å^{-1} was used. The R-factor parameter associated with the goodness of fit for this model was 0.026.

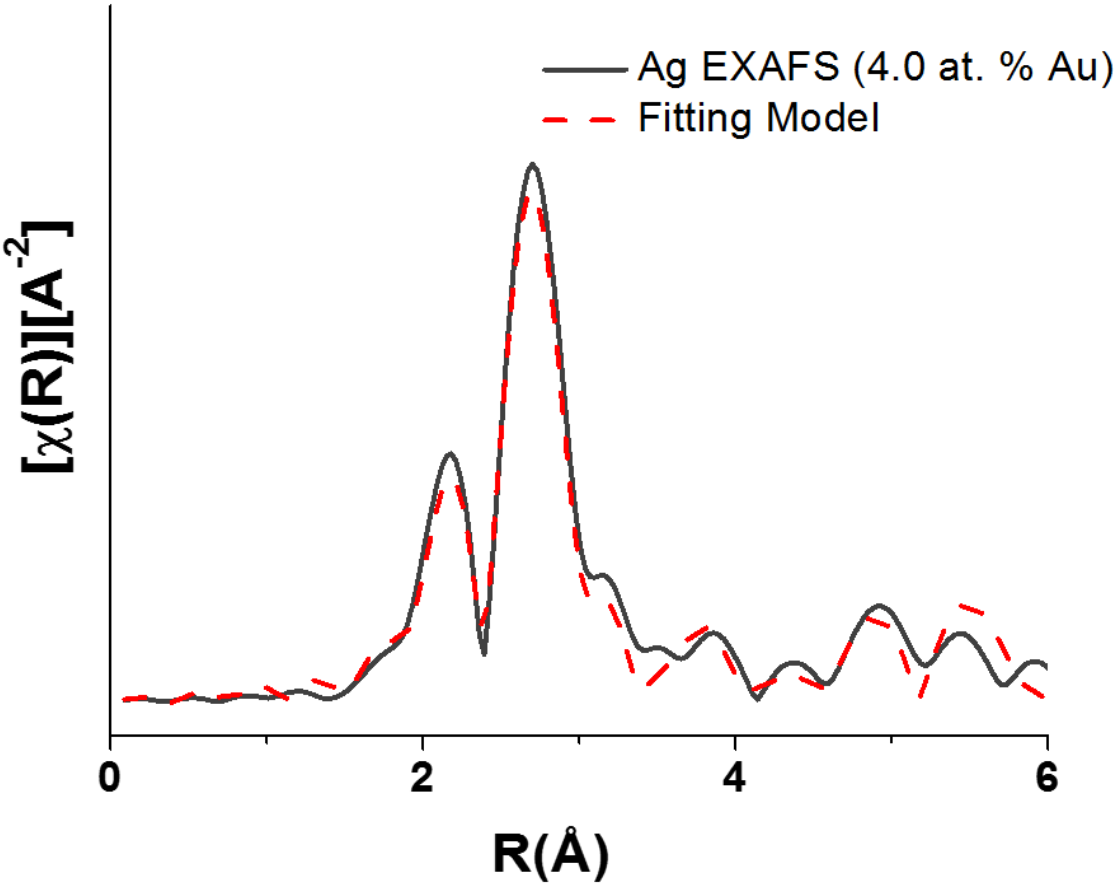

Pathway	N	R (Å)	E_0 (eV)	σ^2 (Å^2) x 10^{-3}
Ag–Ag (shell 1)	11.0 ± 1.0	2.860 ± 0.006	2.6 ± 0.7	8.8 ± 0.7
Ag–Au (shell 1)	1.1 ± 1.0	2.857	1.2 ± 3.5	8.5

Figure S16.4. Ag K edge EXAFS spectrum and fitting model for 4.0 at. % Au nanoparticle sample. The Ag K-edge nanoparticle spectrum was fit using first coordination-shell atomic pathways. Parameters without error bars were fixed based on results from the corresponding Au L3 Edge EXAFS model. A fitting range from 1.5 to 3.5 Å and a k-range from 2 to 12 Å^{-1} was used. The R-factor parameter associated with the goodness of fit for this model was 0.017.

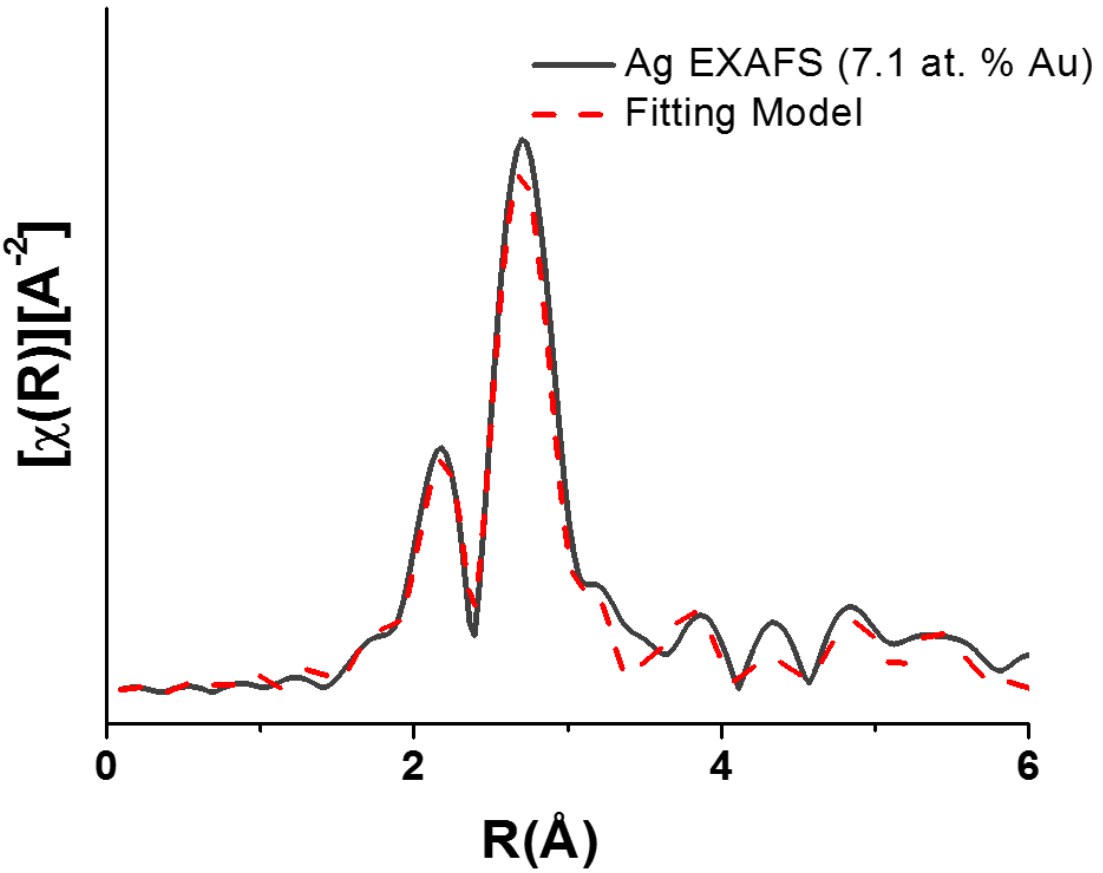

Pathway	N	R (Å)	E_0 (eV)	σ^2 (Å^2) x 10^{-3}
Ag–Ag (shell 1)	11.0 ± 1.3	2.859 ± 0.009	2.8 ± 0.8	8.6 ± 1.2
Ag–Au (shell 1)	1.3 ± 1.1	2.84 ± 0.04	1.3 ± 9.2	7.9 ± 6.5

Figure S16.5. Ag K edge EXAFS spectrum and fitting model for 7.1 at. % Au nanoparticle sample. The Ag K-edge nanoparticle spectrum was fit using first coordination-shell atomic pathways. A fitting range from 1.5 to 3.5 Å and a k-range from 2 to 12 Å^{-1} was used. The R-factor parameter associated with the goodness of fit for this model was 0.020.

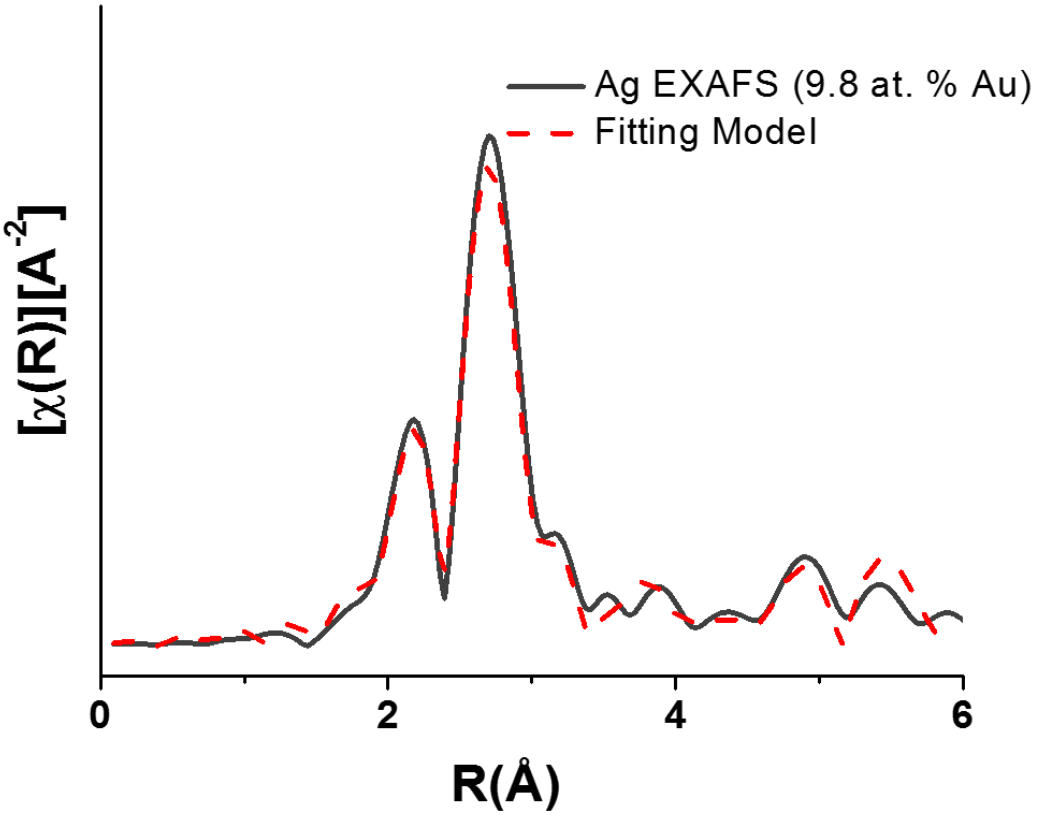

Pathway	N	R (Å)	E_0 (eV)	σ^2 (Å^2) x 10^{-3}
Ag–Ag (shell 1)	10.9 ± 0.9	2.858 ± 0.006	3.1 ± 0.6	8.6 ± 0.6
Ag–Au (shell 1)	1.4 ± 0.9	2.844	1.2 ± 3.7	8.6

Figure S16.6. Ag K edge EXAFS spectrum and fitting model for 9.8 at. % Au nanoparticle sample. The Ag K-edge nanoparticle spectrum was fit using first coordination-shell atomic pathways. Parameters without error bars were fixed based on results from the corresponding Au L3 Edge EXAFS model. A fitting range from 1.5 to 3.5 Å and a k-range from 2 to 12 Å^{-1} was used. The R-factor parameter associated with the goodness of fit for this model was 0.014.

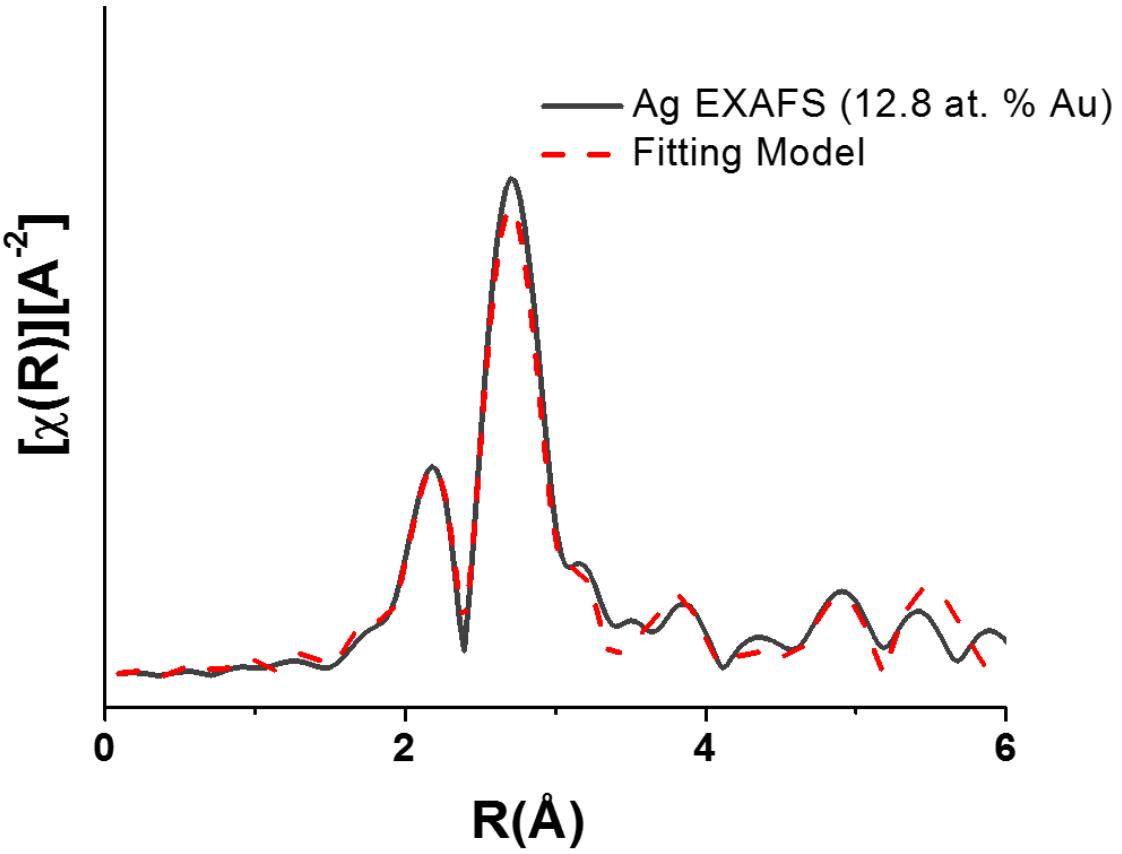

Pathway	N	R (Å)	E_0 (eV)	σ^2 (Å^2) x 10^{-3}
Ag–Ag (shell 1)	10.9 ± 0.8	2.865 ± 0.004	3.2 ± 0.5	8.9 ± 0.5
Ag–Au (shell 1)	1.5 ± 0.6	2.85 ± 0.05	2.7 ± 2.0	9.5 ± 4.0

Figure S16.7. Ag K edge EXAFS spectrum and fitting model for 12.8 at. % Au nanoparticle sample. The Ag K-edge nanoparticle spectrum was fit using first coordination-shell atomic pathways. A fitting range from 1.5 to 3.5 Å and a k-range from 2 to 12 Å^{-1} was used. The R-factor parameter associated with the goodness of fit for this model was 0.014.

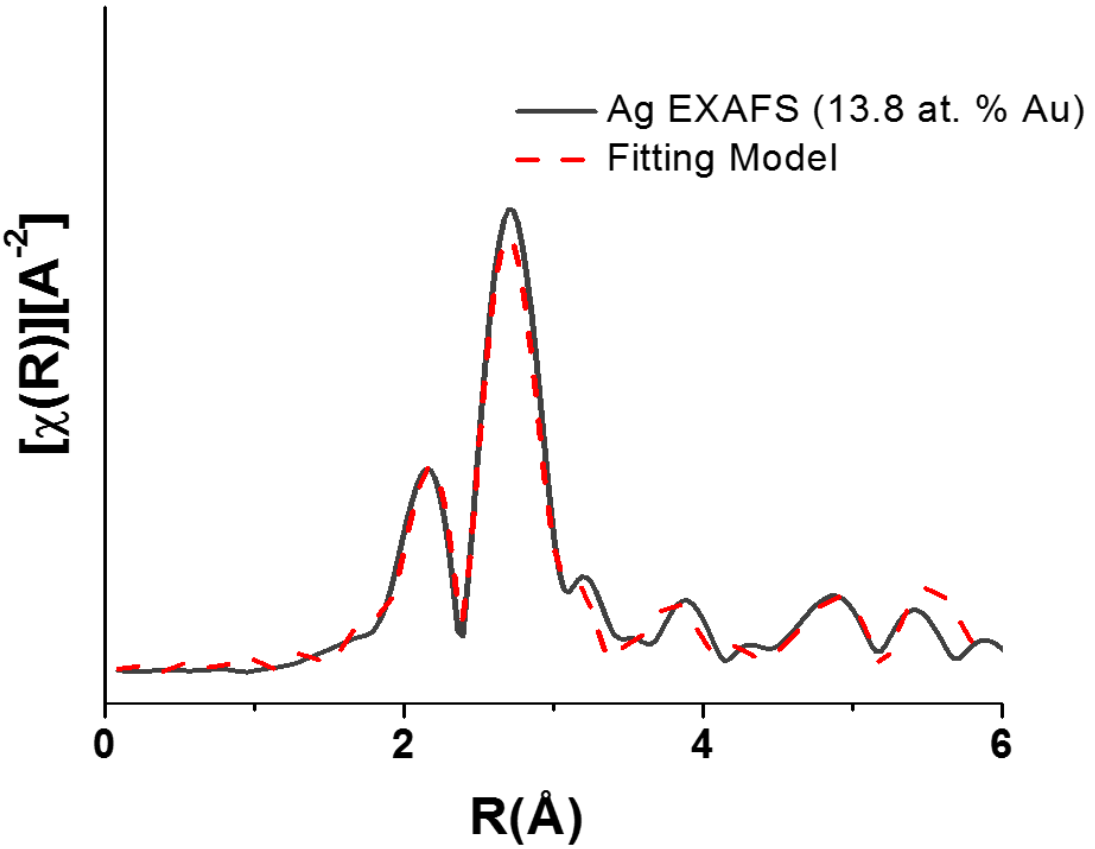

Pathway	N	R (Å)	E_0 (eV)	σ^2 (Å^2) x 10^{-3}
Ag–Ag (shell 1)	10.1 ± 1.3	2.860 ± 0.009	2.1 ± 0.9	9.0 ± 0.9
Ag–Au (shell 1)	2.1 ± 1.3	2.863	1.6 ± 5.5	9.2

Figure S16.8. Ag K edge EXAFS spectrum and fitting model for 13.8 at. % Au nanoparticle sample. The Ag K-edge nanoparticle spectrum was fit using first coordination-shell atomic pathways. Parameters without error bars were fixed based on results from the corresponding Au L3 Edge EXAFS model. A fitting range from 1.5 to 3.5 Å and a k-range from 2 to 12 Å^{-1} was used. The R-factor parameter associated with the goodness of fit for this model was 0.020.

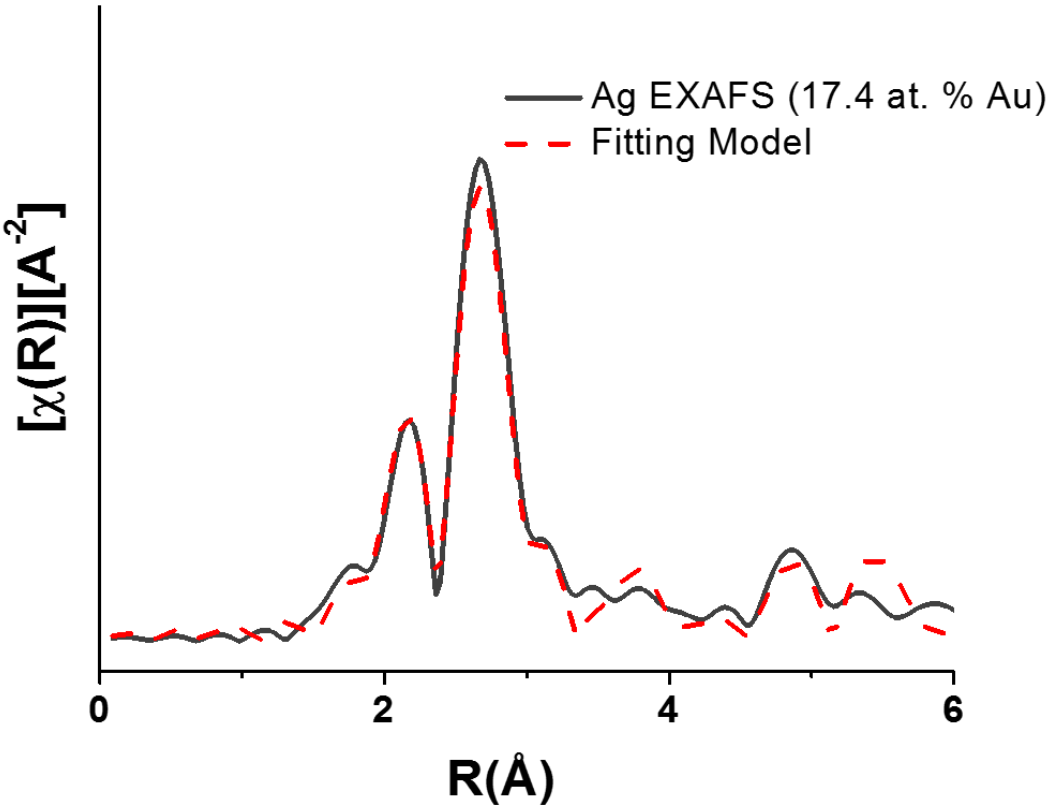

Pathway	N	R (Å)	E_0 (eV)	σ^2 (Å^2) x 10^{-3}
Ag–Ag (shell 1)	10.2 ± 0.9	2.859 ± 0.005	0.8 ± 0.7	7.9 ± 0.6
Ag–Au (shell 1)	2.3 ± 1.1	2.89 ± 0.06	0.5 ± 1.8	7.4 ± 5.0

Figure S16.9. Ag K edge EXAFS spectrum and fitting model for 17.4 at. % Au nanoparticle sample. The Ag K-edge nanoparticle spectrum was fit using first coordination-shell atomic pathways. A fitting range from 1.5 to 3.5 Å and a k-range from 2 to 12 Å^{-1} was used. The R-factor parameter associated with the goodness of fit for this model was 0.015.

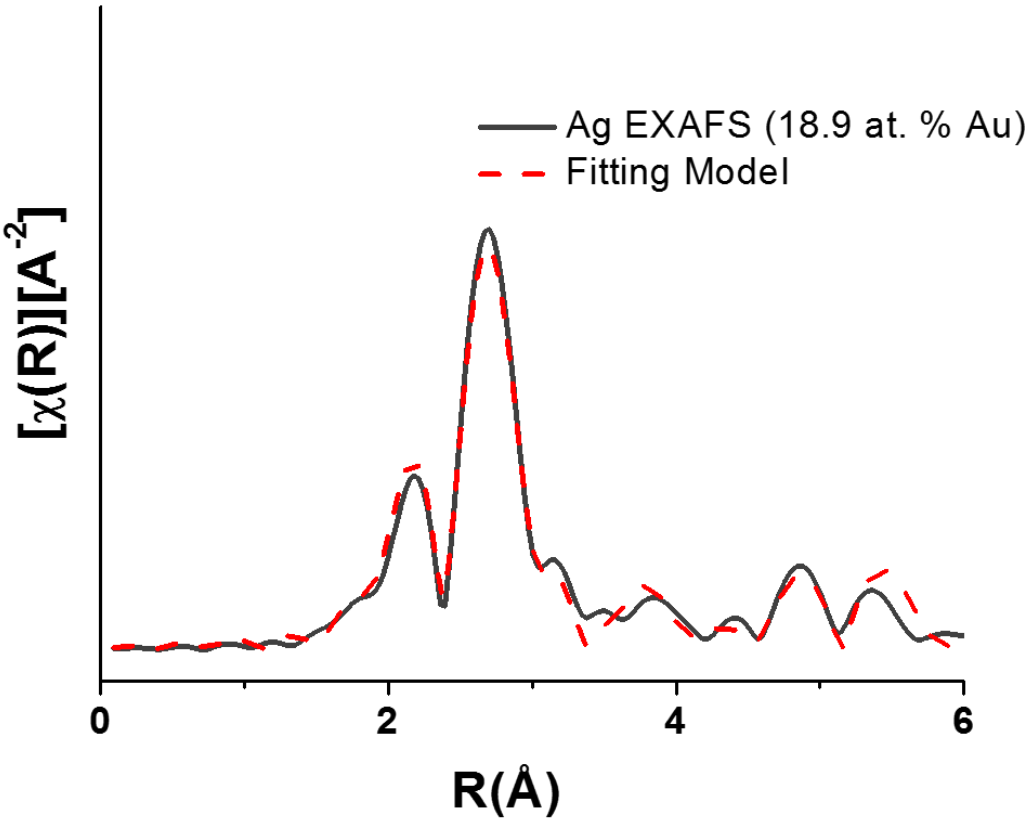

Pathway	N	R (Å)	E_0 (eV)	σ^2 (Å^2) x 10^{-3}
Ag–Ag (shell 1)	9.4 ± 1.0	2.859 ± 0.008	1.3 ± 0.8	8.7 ± 0.8
Ag–Au (shell 1)	1.9 ± 1.0	2.851	0.1 ± 3.8	8.3

Figure S16.10. Ag K edge EXAFS spectrum and fitting model for 18.9 at. % Au nanoparticle sample. The Ag K-edge nanoparticle spectrum was fit using first coordination-shell atomic pathways. Parameters without error bars were fixed based on results from the corresponding Au L3 Edge EXAFS model. A fitting range from 1.5 to 3.5 Å and a k-range from 2 to 12 Å^{-1} was used. The R-factor parameter associated with the goodness of fit for this model was 0.013.

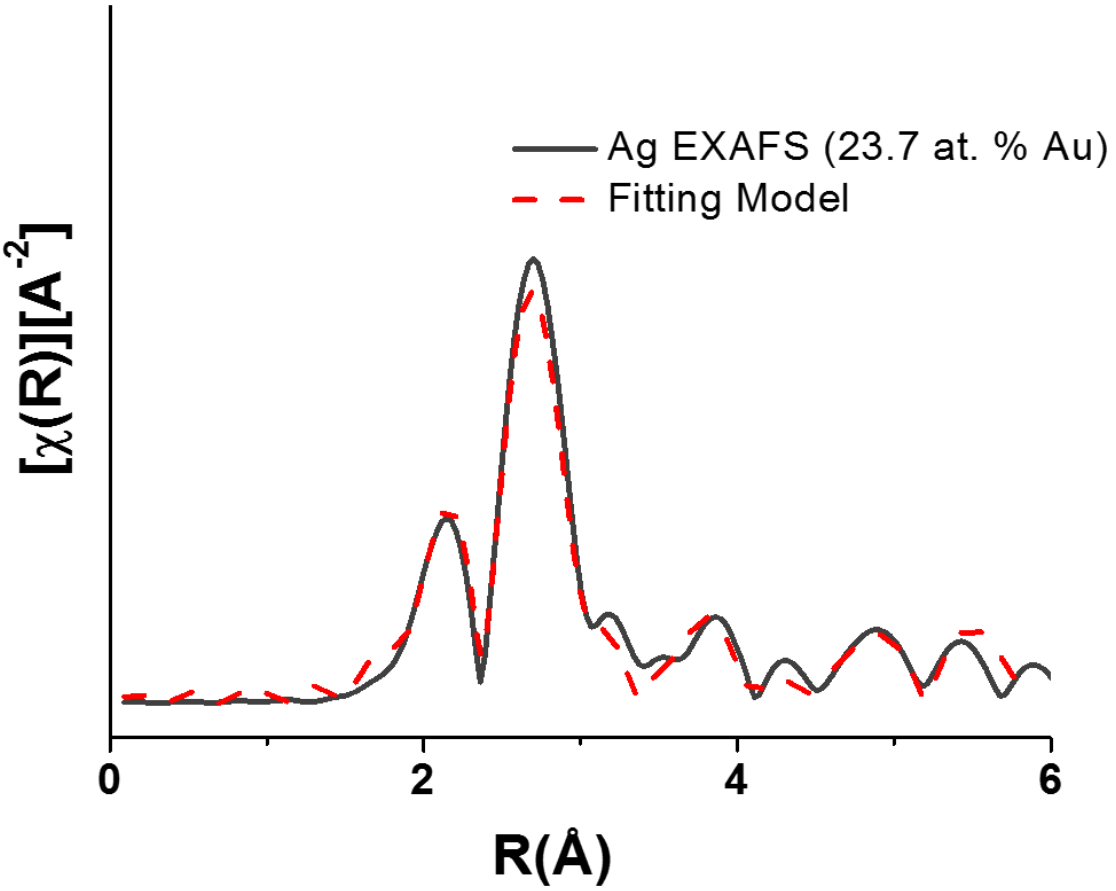

Pathway	N	R (Å)	E_0 (eV)	σ^2 (Å^2) x 10^{-3}
Ag–Ag (shell 1)	9.3 ± 1.1	2.857 ± 0.007	0.9 ± 0.6	9.2 ± 0.9
Ag–Au (shell 1)	2.0 ± 1.1	2.85 ± 0.07	0.2 ± 4.2	8.9 ± 5.0

Figure S16.11. Ag K edge EXAFS spectrum and fitting model for 23.7 at. % Au nanoparticle sample. The Ag K-edge nanoparticle spectrum was fit using first coordination-shell atomic pathways. A fitting range from 1.5 to 3.5 Å and a k-range from 2 to 12 Å^{-1} was used. The R-factor parameter associated with the goodness of fit for this model was 0.021.

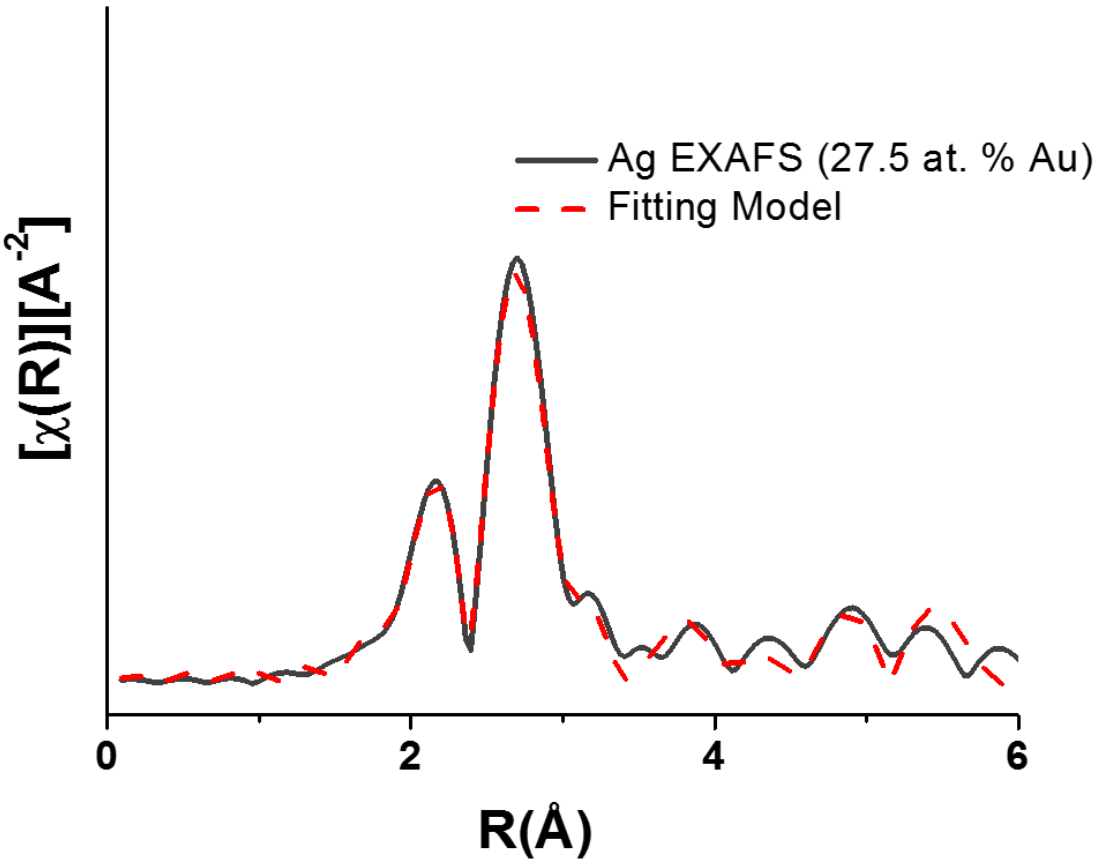

Pathway	N	R (Å)	E_0 (eV)	σ^2 (Å^2) x 10^{-3}
Ag–Ag (shell 1)	9.4 ± 1.1	2.860 ± 0.008	1.2 ± 0.9	8.9 ± 0.9
Ag–Au (shell 1)	2.1 ± 1.0	2.859	-0.1 ± 4.0	7.9

Figure S16.12. Ag K edge EXAFS spectrum and fitting model for 27.5 at. % Au nanoparticle sample. The Ag K-edge nanoparticle spectrum was fit using first coordination-shell atomic pathways. Parameters without error bars were fixed based on results from the corresponding Au L3 Edge EXAFS model. A fitting range from 1.5 to 3.5 Å and a k-range from 2 to 12 Å^{-1} was used. The R-factor parameter associated with the goodness of fit for this model was 0.013.

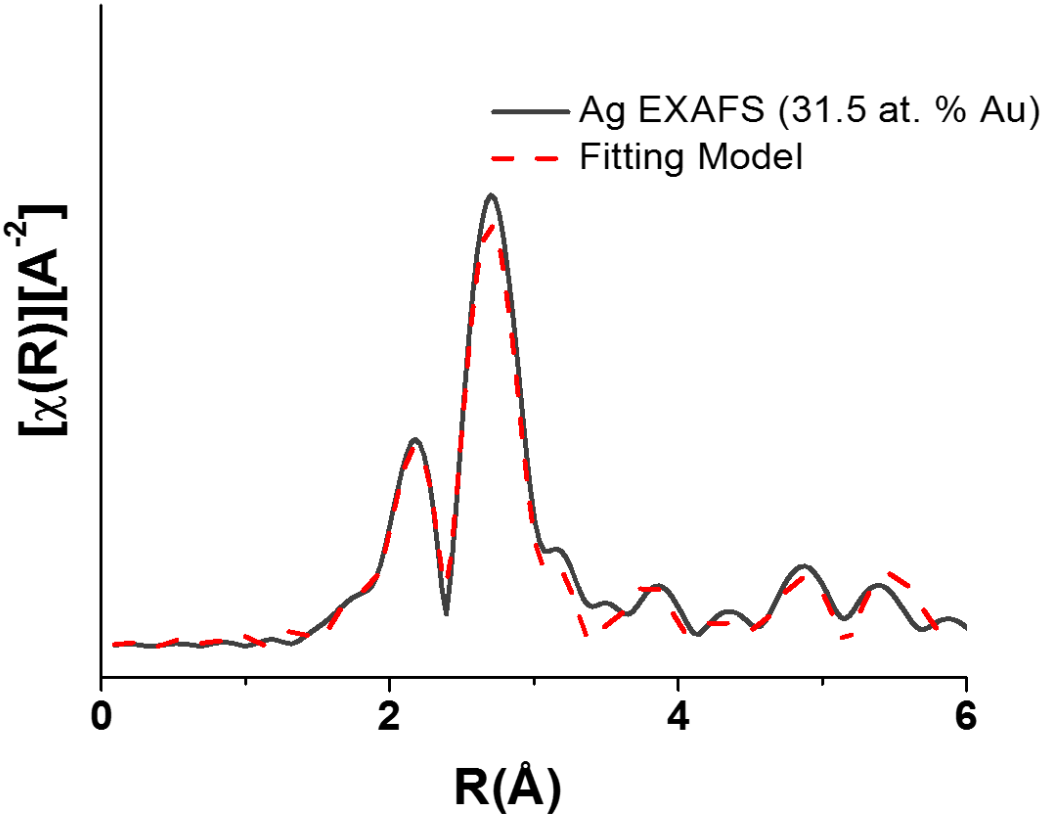

Pathway	N	R (Å)	E_0 (eV)	σ^2 (Å^2) x 10^{-3}
Ag–Ag (shell 1)	9.5 ± 1.0	2.857 ± 0.007	2.1 ± 0.7	8.6 ± 0.7
Ag–Au (shell 1)	2.1 ± 1.0	2.827	-0.3 ± 3.5	7.7

Figure S16.13. Ag K edge EXAFS spectrum and fitting model for 31.5 at. % Au nanoparticle sample. The Ag K-edge nanoparticle spectrum was fit using first coordination-shell atomic pathways. Parameters without error bars were fixed based on results from the corresponding Au L3 Edge EXAFS model. A fitting range from 1.5 to 3.5 Å and a k-range from 2 to 12 Å^{-1} was used. The R-factor parameter associated with the goodness of fit for this model was 0.018.

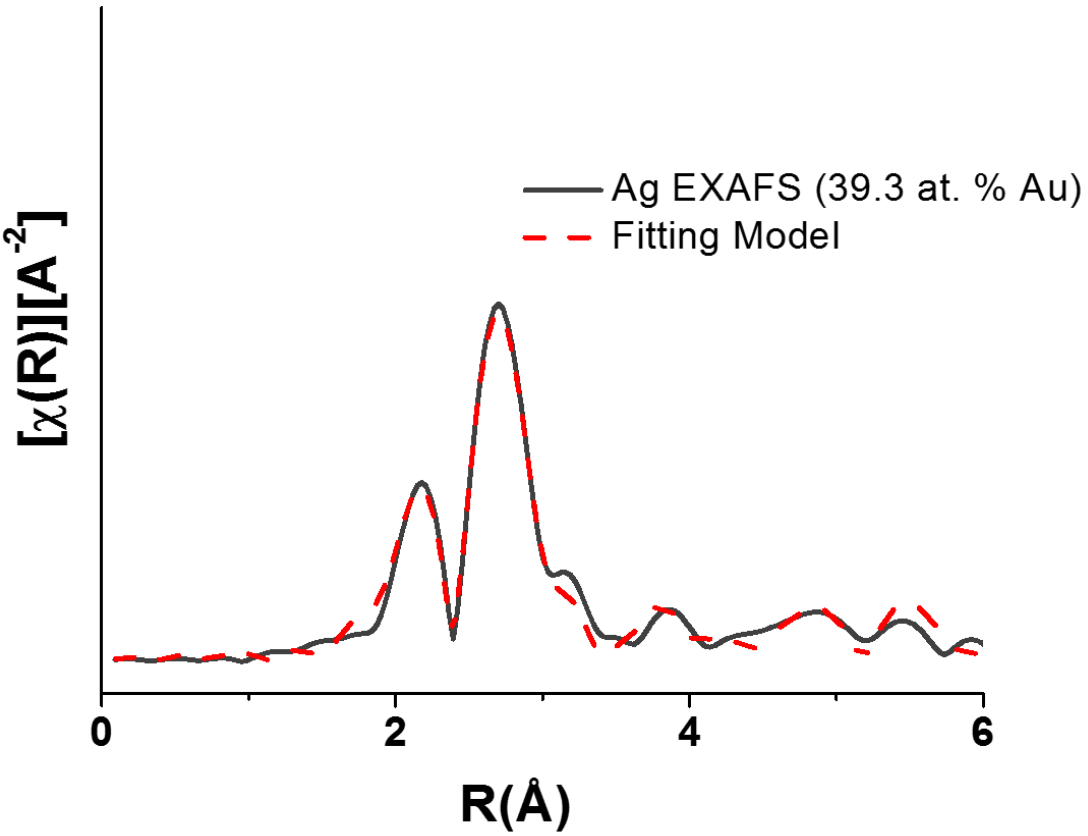

Pathway	N	R (Å)	E_0 (eV)	σ^2 (Å^2) x 10^{-3}
Ag–Ag (shell 1)	8.4 ± 1.1	2.859 ± 0.009	1.4 ± 1.0	9.2 ± 1.0
Ag–Au (shell 1)	2.2 ± 1.0	2.849	0.0 ± 3.6	7.6

Figure S16.14. Ag K edge EXAFS spectrum and fitting model for 39.3 at. % Au nanoparticle sample. The Ag K-edge nanoparticle spectrum was fit using first coordination-shell atomic pathways. Parameters without error bars were fixed based on results from the corresponding Au L3 Edge EXAFS model. A fitting range from 1.5 to 3.5 Å and a k-range from 2 to 12 Å^{-1} was used. The R-factor parameter associated with the goodness of fit for this model was 0.014.

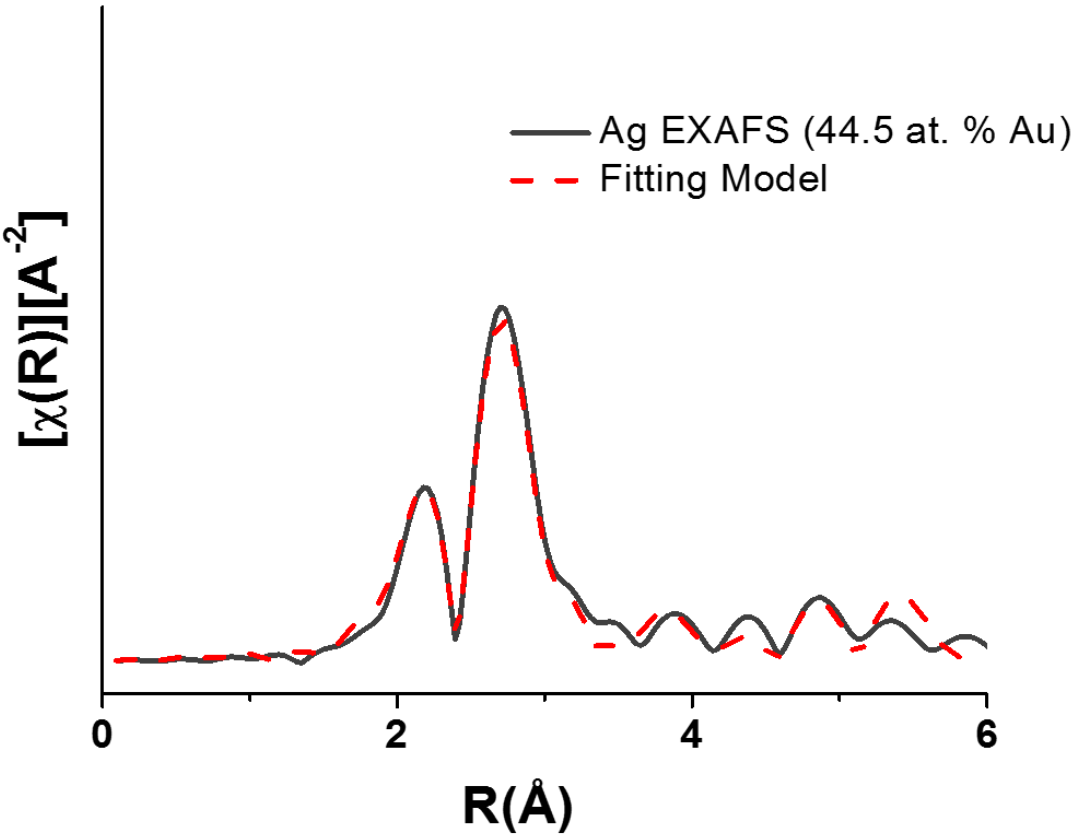

Pathway	N	R (Å)	E_0 (eV)	σ^2 (Å^2) x 10^{-3}
Ag–Ag (shell 1)	8.2 ± 1.0	2.860 ± 0.009	1.7 ± 0.9	9.3 ± 0.9
Ag–Au (shell 1)	2.6 ± 1.0	2.845	0.3 ± 3.1	7.9

Figure S16.15. Ag K edge EXAFS spectrum and fitting model for 44.5 at. % Au nanoparticle sample. The Ag K-edge nanoparticle spectrum was fit using first coordination-shell atomic pathways. Parameters without error bars were fixed based on results from the corresponding Au L3 Edge EXAFS model. A fitting range from 1.5 to 3.5 Å and a k-range from 2 to 12 Å^{-1} was used. The R-factor parameter associated with the goodness of fit for this model was 0.014.

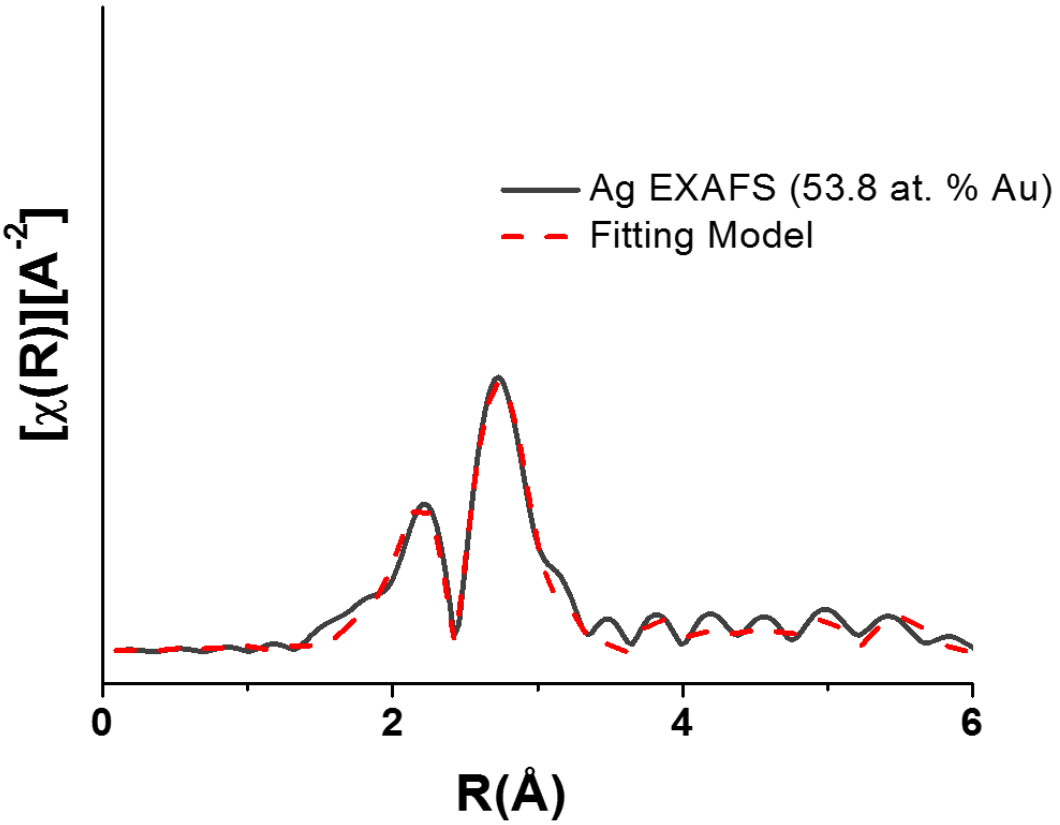

Pathway	N	R (Å)	E_0 (eV)	σ^2 (Å^2) x 10^{-3}
Ag–Ag (shell 1)	6.7 ± 1.1	2.86 ± 0.01	1.8 ± 1.4	9.9 ± 1.4
Ag–Au (shell 1)	3.1 ± 1.0	2.846	0.3 ± 2.6	8.3

Figure S16.16. Ag K edge EXAFS spectrum and fitting model for 53.8 at. % Au nanoparticle sample. The Ag K-edge nanoparticle spectrum was fit using first coordination-shell atomic pathways. Parameters without error bars were fixed based on results from the corresponding Au L3 Edge EXAFS model. A fitting range from 1.5 to 3.5 Å and a k-range from 2 to 12 Å^{-1} was used. The R-factor parameter associated with the goodness of fit for this model was 0.023.

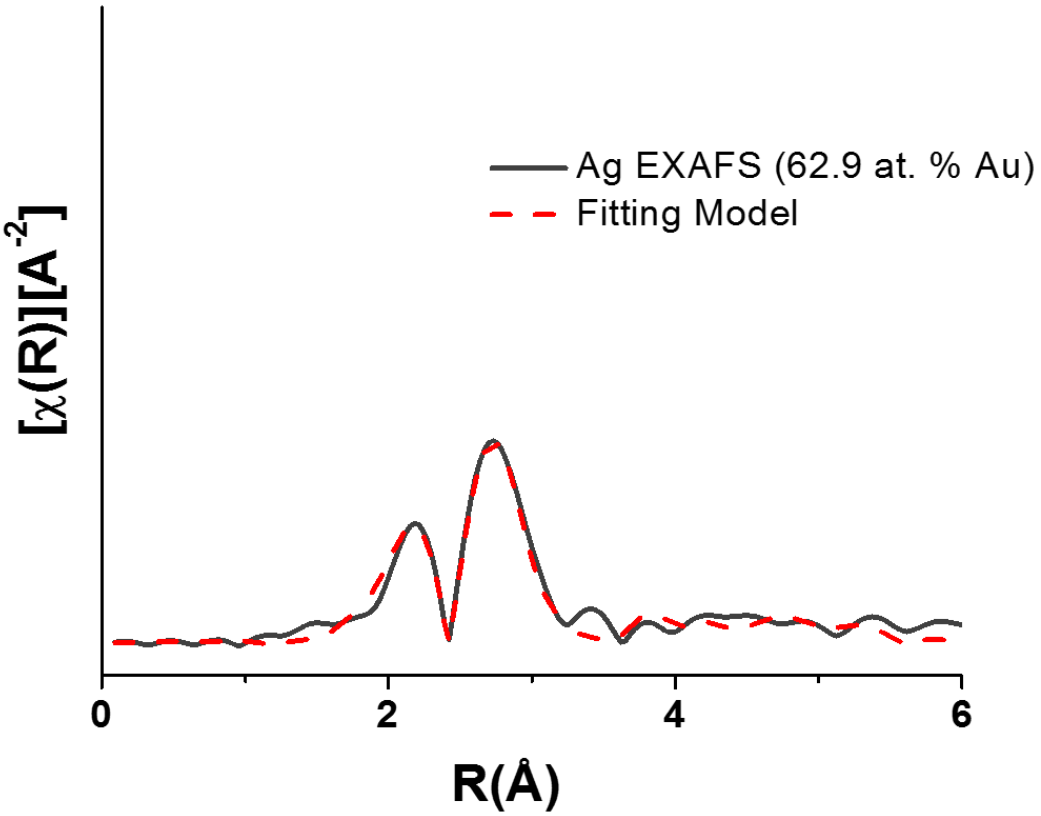

Pathway	N	R (Å)	E_0 (eV)	σ^2 (Å^2) x 10^{-3}
Ag–Ag (shell 1)	5.6 ± 1.0	2.86 ± 0.02	0.1 ± 1.5	10.7 ± 1.6
Ag–Au (shell 1)	3.2 ± 0.9	2.848	-0.2 ± 2.4	8.5

Figure S16.17. Ag K edge EXAFS spectrum and fitting model for 62.9 at. % Au nanoparticle sample. The Ag K-edge nanoparticle spectrum was fit using first coordination-shell atomic pathways. Parameters without error bars were fixed based on results from the corresponding Au L3 Edge EXAFS model. A fitting range from 1.5 to 3.5 Å and a k-range from 2 to 12 Å^{-1} was used. The R-factor parameter associated with the goodness of fit for this model was 0.024.

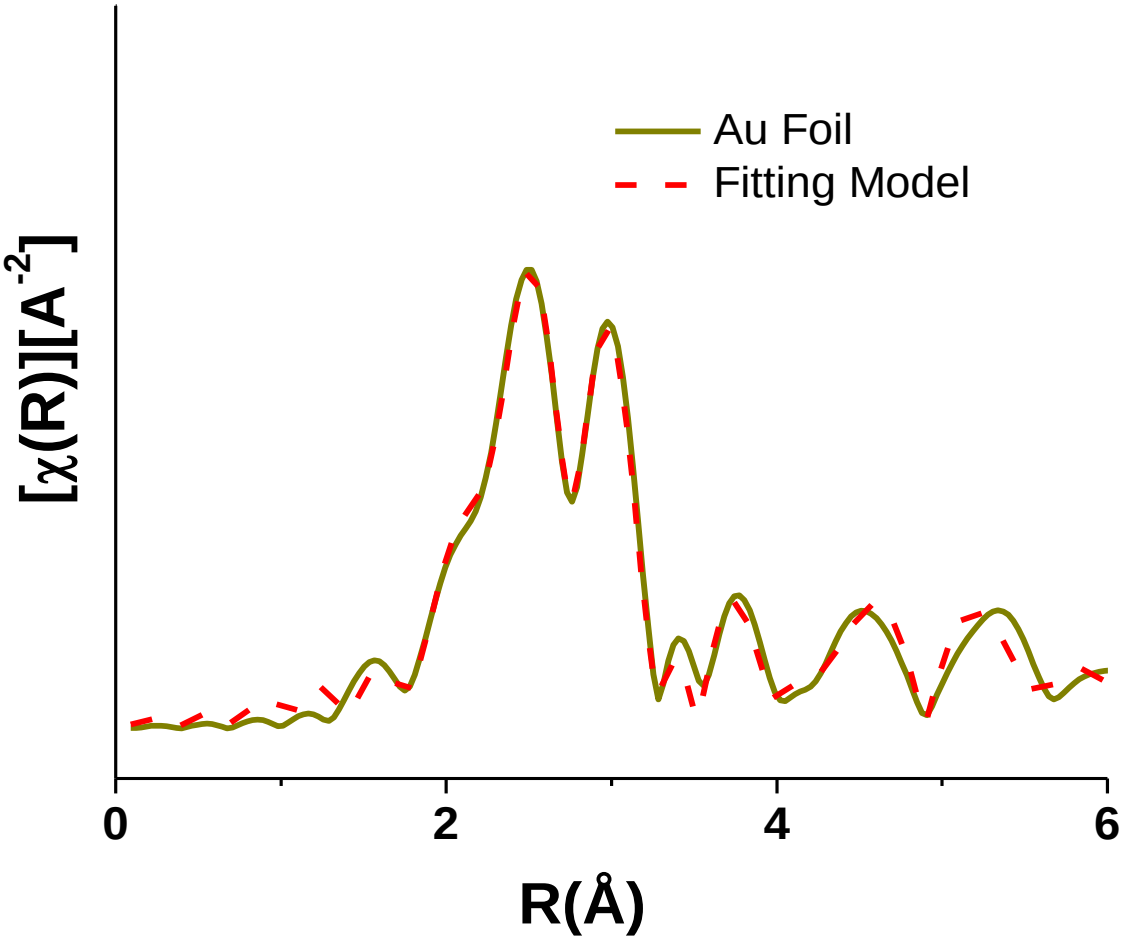

Pathway	N_{theory}	S_0^2	R (Å)	E_0 (eV)	σ^2 (Å^2) x 10^{-3}
Au–Au (shell 1)	12	0.75	2.861	5.11	7.71
Au–Au (shell 2)	6	0.75	4.051	5.11	10.8
Au–Au (shell 3)	24	0.75	4.986	5.11	12.0

Figure S16.18. Au L_3 edge Au foil EXAFS standard and fitting model. Au foil data was collected and modeled in order to determine the amplitude reduction factor (S_0^2), since the coordination number is a fixed known. A fitting range from 1.5 to 5 Å and a k-range from 2 to 12 Å^{-1} was used. The R-factor parameter associated with the goodness of fit for this model was 0.009.

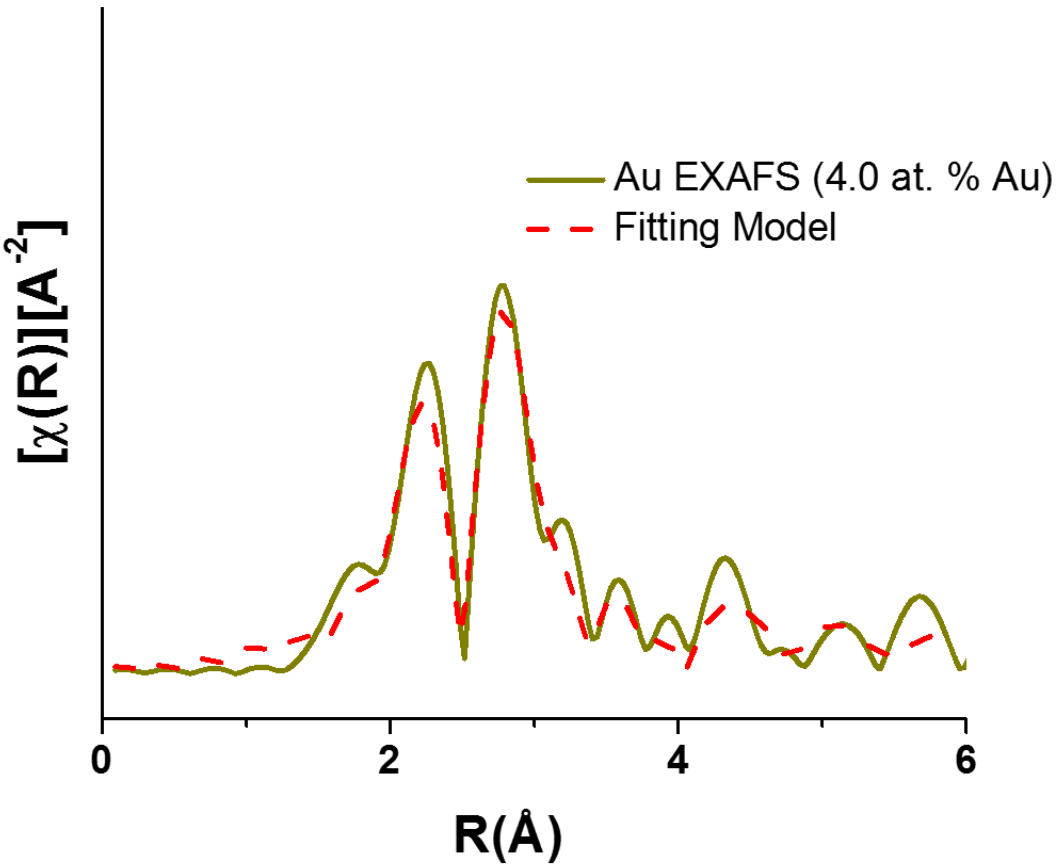

Pathway	N	R (Å)	E_0 (eV)	σ^2 (Å^2) x 10^{-3}
Au–Au (shell 1)	4.8 ± 1.3	2.88 ± 0.02	3.1 ± 0.9	10.2 ± 4.0
Au–Ag (shell 1)	6.4 ± 0.8	2.857 ± 0.009	5.0 ± 1.3	8.5 ± 1.1

Figure S16.19. Au L3 edge EXAFS spectrum and fitting model for 4.0 at. % Au nanoparticle sample. The Au L3-edge nanoparticle spectrum was fit using first coordination-shell atomic pathways. A fitting range from 1.5 to 3.5 Å and a k-range from 2 to 12 Å^{-1} was used. The R-factor parameter associated with the goodness of fit for this model was 0.052.

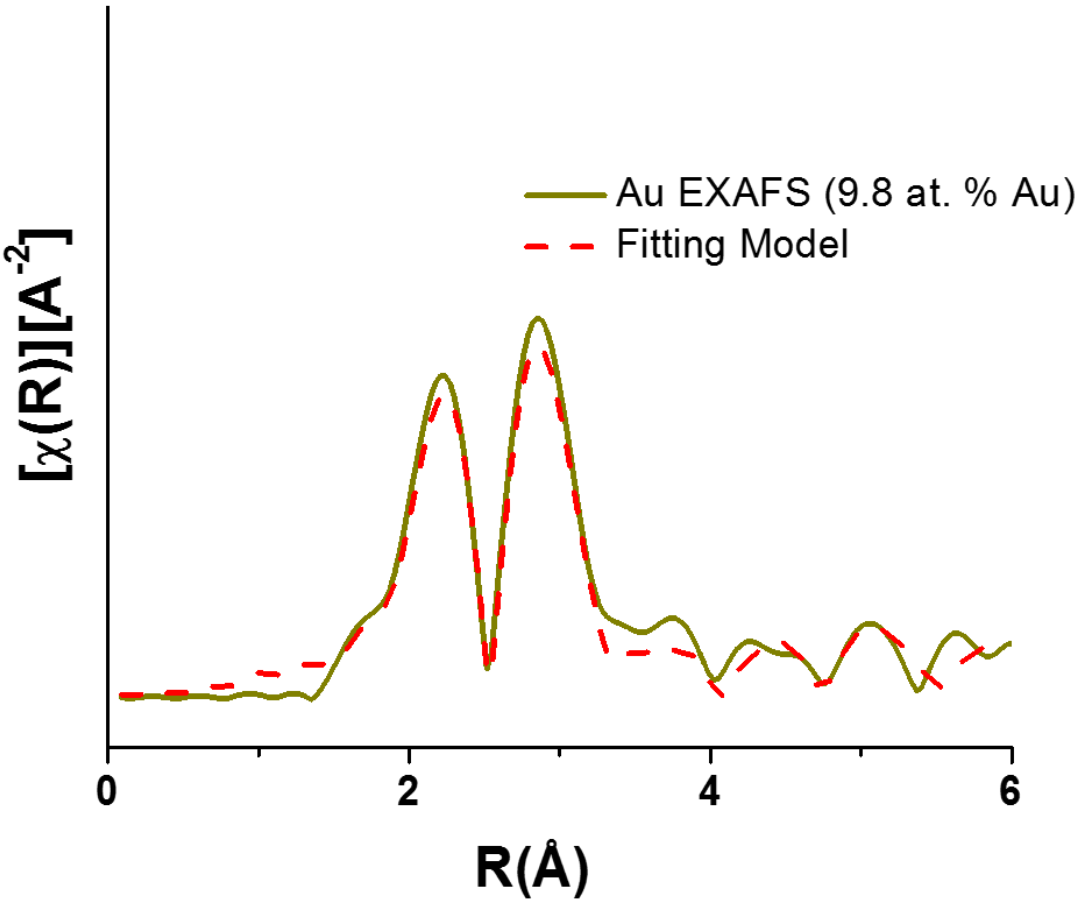

Pathway	N	R (Å)	E_0 (eV)	σ^2 (Å^2) x 10^{-3}
Au–Au (shell 1)	6.2 ± 1.6	2.86 ± 0.01	3.7 ± 1.1	7.9 ± 2.2
Au–Ag (shell 1)	5.8 ± 0.9	2.84 ± 0.01	3.9 ± 1.2	8.6 ± 1.4

Figure S16.20. Au L3 edge EXAFS spectrum and fitting model for 9.8 at. % Au nanoparticle sample. The Au L3-edge nanoparticle spectrum was fit using first coordination-shell atomic pathways. A fitting range from 1.5 to 3.5 Å and a k-range from 2 to 12 Å^{-1} was used. The R-factor parameter associated with the goodness of fit for this model was 0.022.

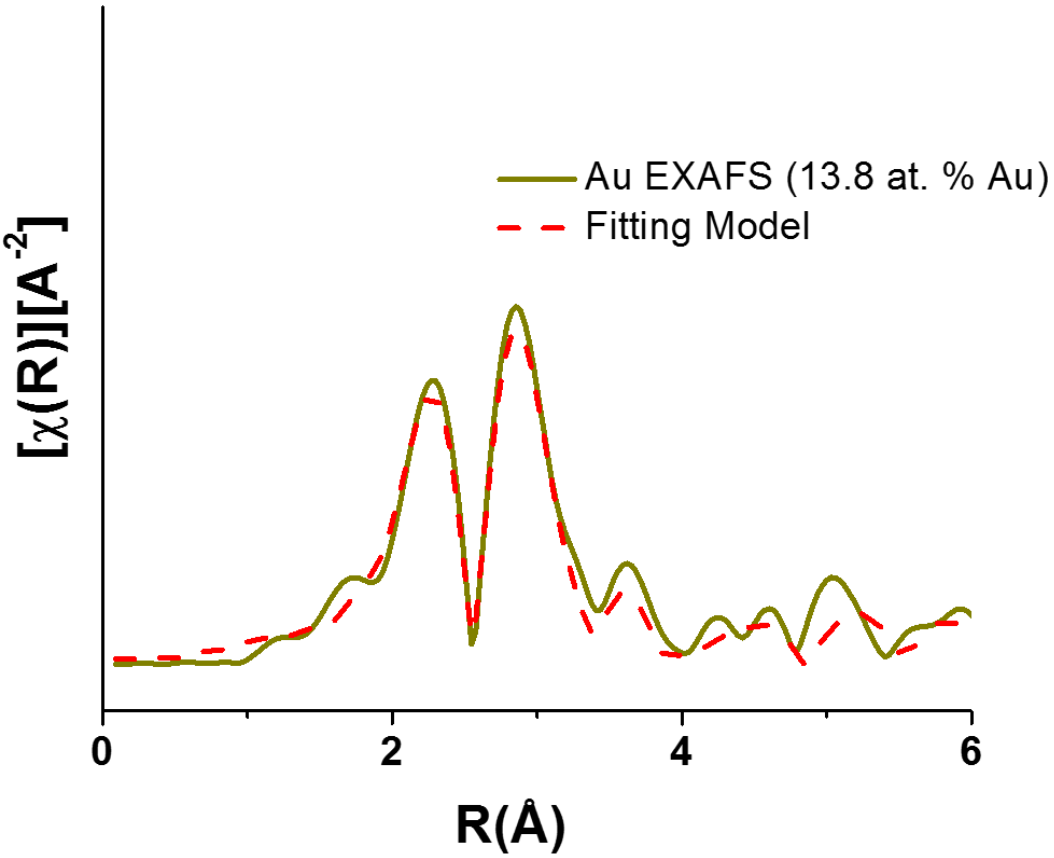

Pathway	N	R (Å)	E_0 (eV)	σ^2 (Å^2) x 10^{-3}
Au–Au (shell 1)	6.4 ± 1.5	2.86 ± 0.02	3.9 ± 0.9	9.5 ± 4.0
Au–Ag (shell 1)	5.5 ± 0.9	2.86 ± 0.01	4.7 ± 1.2	9.1 ± 1.2

Figure S16.21. Au L3 edge EXAFS spectrum and fitting model for 13.8 at. % Au nanoparticle sample. The Au L3-edge nanoparticle spectrum was fit using first coordination-shell atomic pathways. A fitting range from 1.5 to 3.5 Å and a k-range from 2 to 12 Å^{-1} was used. The R-factor parameter associated with the goodness of fit for this model was 0.022.

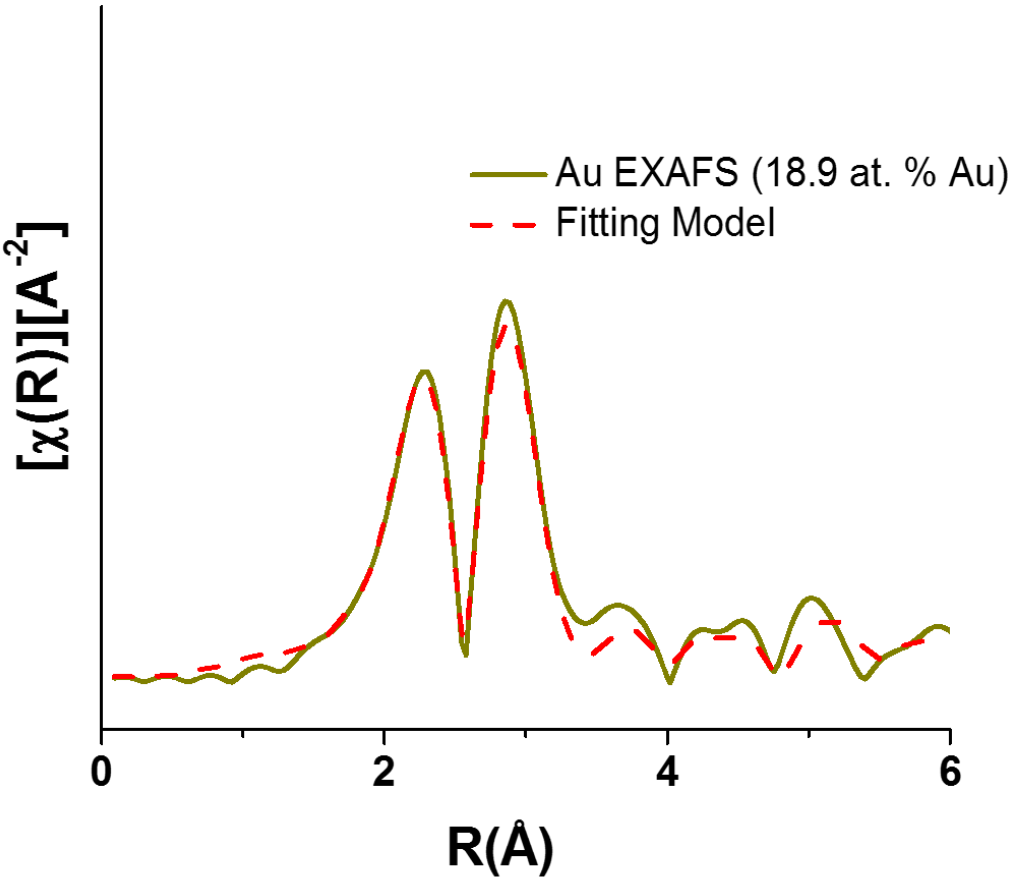

Pathway	N	R (Å)	E_0 (eV)	σ^2 (Å^2) x 10^{-3}
Au–Au (shell 1)	6.8 ± 1.3	2.847 ± 0.009	3.7 ± 0.7	8.1 ± 2.0
Au–Ag (shell 1)	5.0 ± 0.9	2.85 ± 0.01	4.4 ± 0.9	8.3 ± 1.0

Figure S16.22. Au L3 edge EXAFS spectrum and fitting model for 18.9 at. % Au nanoparticle sample. The Au L3-edge nanoparticle spectrum was fit using first coordination-shell atomic pathways. A fitting range from 1.5 to 3.5 Å and a k-range from 2 to 12 Å^{-1} was used. The R-factor parameter associated with the goodness of fit for this model was 0.011.

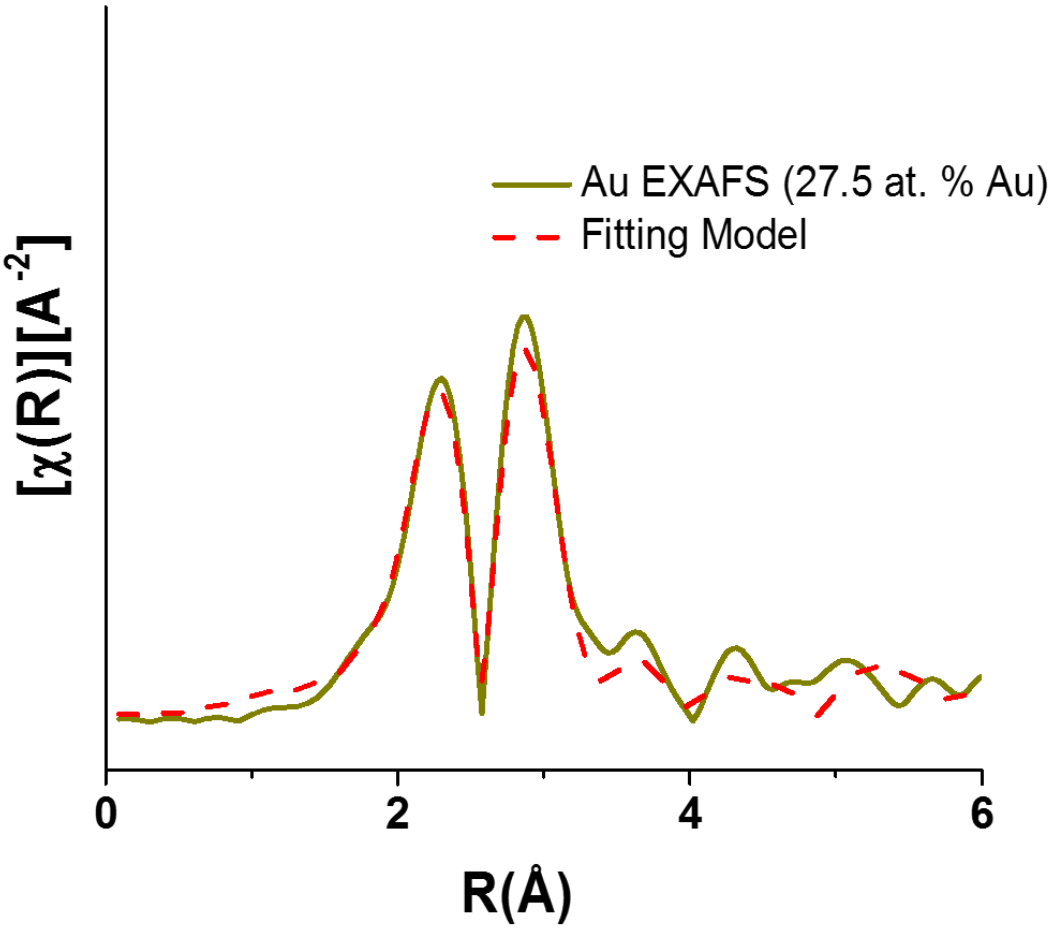

Pathway	N	R (Å)	E_0 (eV)	σ^2 (Å^2) x 10^{-3}
Au–Au (shell 1)	6.9 ± 2.1	2.85 ± 0.01	3.5 ± 0.8	8.1 ± 2.8
Au–Ag (shell 1)	4.8 ± 0.7	2.86 ± 0.01	5.3 ± 1.1	7.9 ± 1.1

Figure S16.23. Au L3 edge EXAFS spectrum and fitting model for 27.5 at. % Au nanoparticle sample. The Au L3-edge nanoparticle spectrum was fit using first coordination-shell atomic pathways. A fitting range from 1.5 to 3.5 Å and a k-range from 2 to 12 Å^{-1} was used. The R-factor parameter associated with the goodness of fit for this model was 0.017.

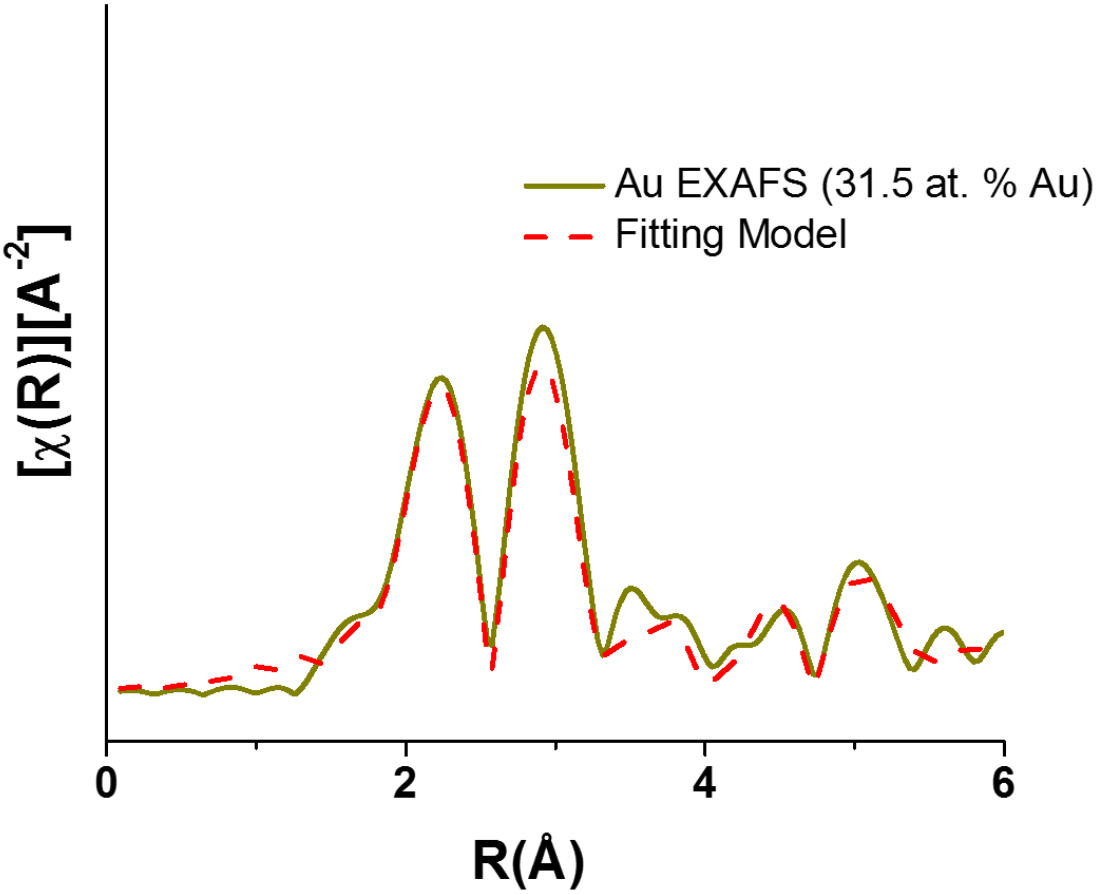

Pathway	N	R (Å)	E_0 (eV)	σ^2 (Å^2) x 10^{-3}
Au–Au (shell 1)	7.2 ± 1.1	2.847 ± 0.007	4.1 ± 0.8	7.2 ± 1.4
Au–Ag (shell 1)	4.5 ± 0.7	2.83 ± 0.01	3.6 ± 1.1	7.7 ± 1.3

Figure S16.24. Au L3 edge EXAFS spectrum and fitting model for 31.5 at. % Au nanoparticle sample. The Au L3-edge nanoparticle spectrum was fit using first coordination-shell atomic pathways. A fitting range from 1.5 to 3.5 Å and a k-range from 2 to 12 Å^{-1} was used. The R-factor parameter associated with the goodness of fit for this model was 0.018.

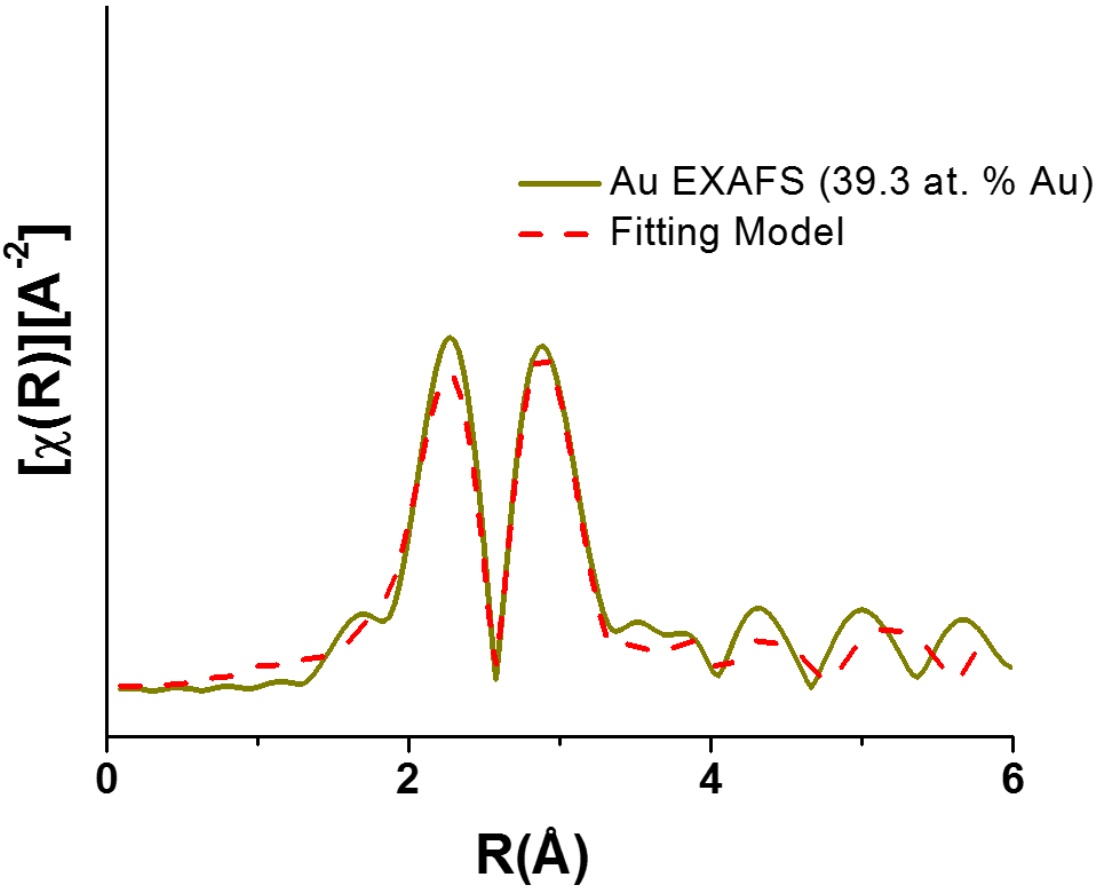

Pathway	N	R (Å)	E_0 (eV)	σ^2 (Å^2) x 10^{-3}
Au–Au (shell 1)	7.4 ± 1.3	2.854 ± 0.008	3.7 ± 0.9	7.9 ± 1.6
Au–Ag (shell 1)	4.5 ± 0.6	2.849 ± 0.009	4.3 ± 1.2	7.6 ± 1.1

Figure S16.25. Au L3 edge EXAFS spectrum and fitting model for 39.3 at. % Au nanoparticle sample. The Au L3-edge nanoparticle spectrum was fit using first coordination-shell atomic pathways. A fitting range from 1.5 to 3.5 Å and a k-range from 2 to 12 Å^{-1} was used. The R-factor parameter associated with the goodness of fit for this model was 0.013.

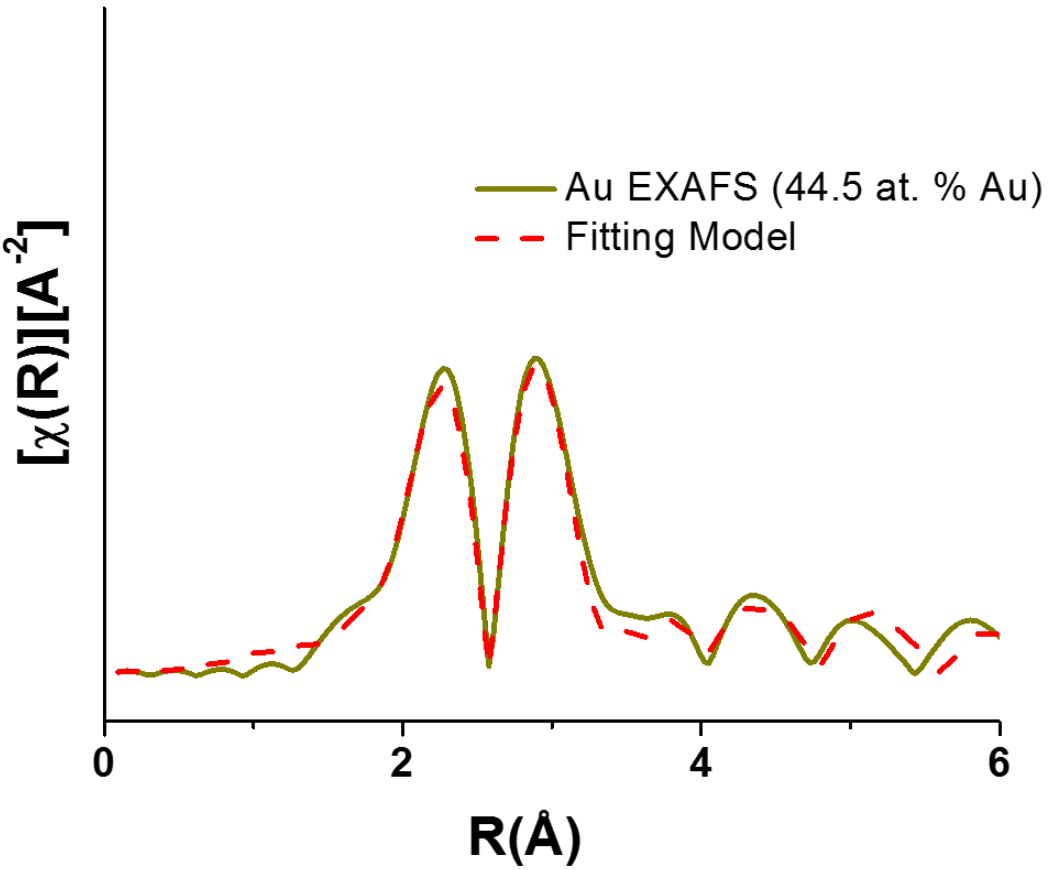

Pathway	N	R (Å)	E_0 (eV)	σ^2 (Å^2) x 10^{-3}
Au–Au (shell 1)	7.4 ± 1.2	2.854 ± 0.006	3.7 ± 0.6	8.2 ± 1.3
Au–Ag (shell 1)	4.3 ± 0.4	2.845 ± 0.008	3.8 ± 0.9	7.9 ± 0.9

Figure S16.26. Au L3 edge EXAFS spectrum and fitting model for 44.5 at. % Au nanoparticle sample. The Au L3-edge nanoparticle spectrum was fit using first coordination-shell atomic pathways. A fitting range from 1.5 to 3.5 Å and a k-range from 2 to 12 Å^{-1} was used. The R-factor parameter associated with the goodness of fit for this model was 0.017.

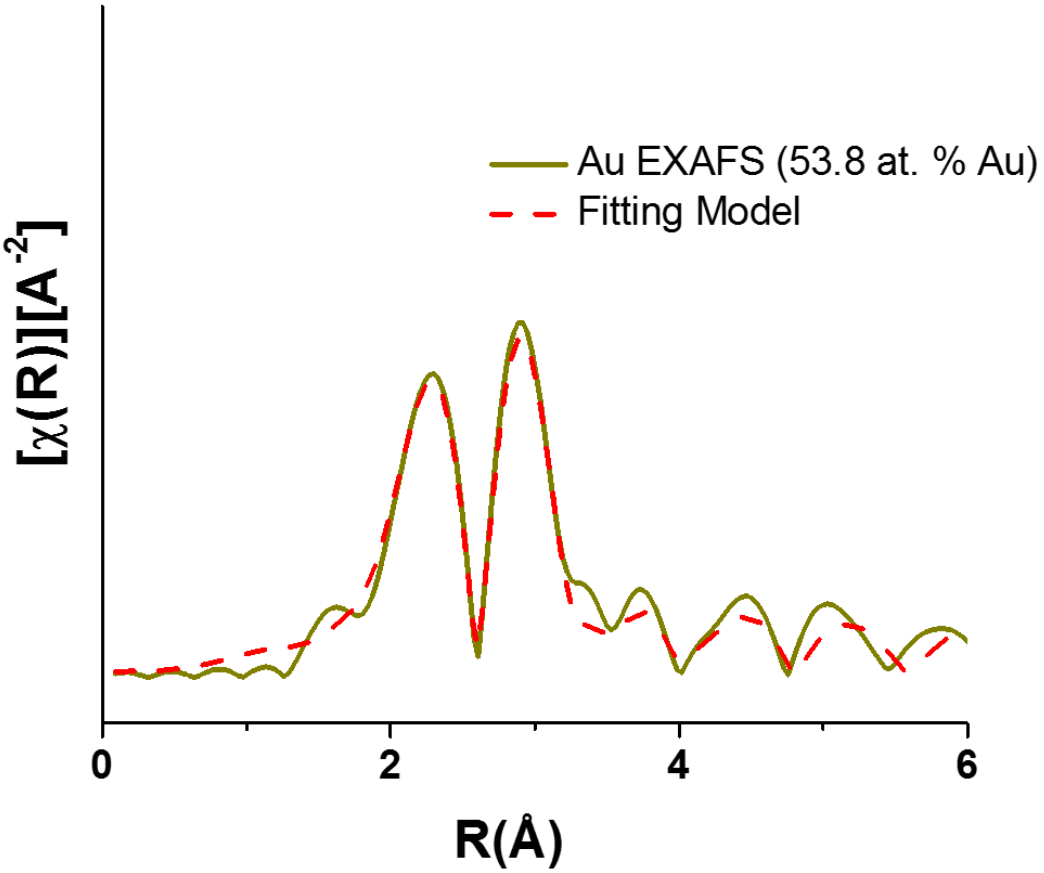

Pathway	N	R (Å)	E_0 (eV)	σ^2 (Å^2) x 10^{-3}
Au–Au (shell 1)	7.7 ± 1.4	2.84 ± 0.01	3.9 ± 1.0	8.0 ± 1.9
Au–Ag (shell 1)	4.2 ± 0.8	2.85 ± 0.02	4.5 ± 1.6	8.3 ± 1.8

Figure S16.27. Au L3 edge EXAFS spectrum and fitting model for 53.8 at. % Au nanoparticle sample. The Au L3-edge nanoparticle spectrum was fit using first coordination-shell atomic pathways. A fitting range from 1.5 to 3.5 Å and a k-range from 2 to 12 Å^{-1} was used. The R-factor parameter associated with the goodness of fit for this model was 0.011.

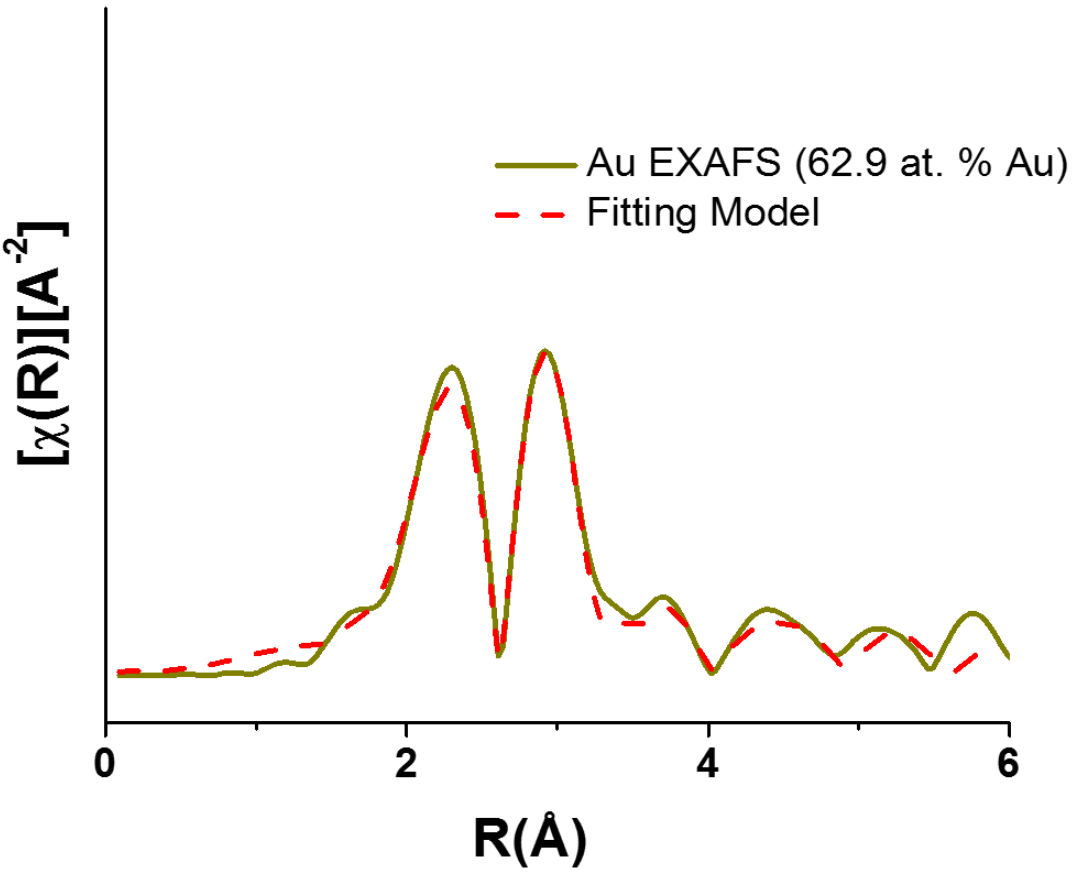

Pathway	N	R (Å)	E_0 (eV)	σ^2 (Å^2) x 10^{-3}
Au–Au (shell 1)	8.1 ± 1.1	2.851 ± 0.006	4.1 ± 0.6	8.2 ± 1.3
Au–Ag (shell 1)	4.0 ± 0.5	2.85 ± 0.01	4.5 ± 1.3	8.5 ± 1.3

Figure S16.28. Au L3 edge EXAFS spectrum and fitting model for 62.9 at. % Au nanoparticle sample. The Au L3-edge nanoparticle spectrum was fit using first coordination-shell atomic pathways. A fitting range from 1.5 to 3.5 Å and a k-range from 2 to 12 Å^{-1} was used. The R-factor parameter associated with the goodness of fit for this model was 0.011.

References

1. Puri, S.; Chand, B.; Mehta, D.; Garg, M. L.; Singh, N.; Trehan, P. N., *Atomic Data and Nuclear Data Tables* **1995,** *61,* 289-311.
2. Guinier, A.; Fournet, G., *Small-Angle Scattering of X-Rays*. John Wiley and Sons: New York, 1955.
3. Als-Nielsen, J. M., D., *Elements of Modern X-Ray Physics*. 2 ed.; John Wiley: Chichester, U.K., 2011.

4. Ravel, B.; Newville, M., *J. Synchrotron Radiat.* **2005,** *12,* 537-541.
5. Ravel, B., *J. Synchrotron Radiat.* **2001,** *8,* 314-316.
6. Ravel, B.; Newville, M.; Cross, J. O.; Bouldin, C. E., *Physica B* **1995,** *208 & 209,* 145-7.
7. Stern, E. A., *Contemp. Phys.* **1978,** *19,* 289-310.
8. Stern, E. A., *Phys. Rev. B* **1974,** *10,* 3027-37.
9. Ravel, B.; Kelly, S. D., *AIP Conf. Proc.* **2007,** *882,* 150-152.
10. Scott, R., *Physical Methods in Bioinorganic Chemistry: Spectroscopy and Magnetism*. University Science Books: 2000.
11. Michalowicz, A.; Vlaic, G., *J. Synchrotron Radiat.* **1998,** *5,* 1317-1320.
12. Calvin, S.; Miller, M. M.; Goswami, R.; Cheng, S.-F.; Mulvaney, S. P.; Whitman, L. J.; Harris, V. G., *Journal of Applied Physics* **2003,** *94,* 778-783.